Rapid #: -1194008 **Ariel IP: 128.223.84.143**

2

CALL #:	**QC801 .R46**
LOCATION:	**LDL :: Main Library :: Geology**
TYPE:	Article CC:CCL
JOURNAL TITLE:	Reviews of geophysics
USER JOURNAL TITLE:	
LDL CATALOG TITLE:	Reviews of geophysics
ARTICLE TITLE:	kamb,b "sliding motion of glaciers: theory and observation"
ARTICLE AUTHOR:	
VOLUME:	86
ISSUE:	-
MONTH:	
YEAR:	1970
PAGES:	673-728
ISSN:	0096-1043
OCLC #:	1900020
CROSS REFERENCE ID:	30849901
VERIFIED:	

BORROWER:	**ORU :: Main Library**
PATRON:	**Rempel, Alan William**
PATRON ID:	.p1201930
PATRON ADDRESS:	
PATRON PHONE:	
PATRON FAX:	
PATRON E-MAIL:	-
PATRON DEPT:	none
PATRON STATUS:	PTYPE:2
PATRON NOTES:	

RAPID

System Date/Time: 5/18/2007 3:17:39 PM MST

COPY

Rapid Updated

MAY 21 2007

Scanned / Sent

Published quarterly by the American Geophysical Union from 2901 Byrdhill Road, Richmond, Virginia 23205. Second-class postage paid at Richmond, Virginia.

Subscriptions, orders for back numbers, and changes of address should be sent to American Geophysical Union, Suite 435, 2100 Pennsylvania Avenue, N.W., Washington, D. C. 20037. Library and nonmember subscription $12.50 per year. (Available to members as a subscription option.) Single-copy price $5.00.

Sliding Motion of Glaciers: Theory and Observation

BARCLAY KAMB

Division of Geological Sciences
California Institute of Technology, Pasadena, California 91109

Abstract. The sliding motion of glacier ice over bedrock, which contributes about half the flow velocity of temperate glaciers, is analyzed for arbitrary bedrock topography of low roughness. Fourier-analyzed topography is represented by a roughness spectral function $\zeta(h, k)$ defined in terms of the mean square topographic amplitude. From an essentially exact solution of the sliding problem for linear ice-flow rheology, an approximate solution for the actual nonlinear rheology is built on the assumption that the second strain-rate invariant depends only on distance from the ice-bedrock contact. The transition wavelength λ_s between regelation and plastic flow, constant in the linear theory, is replaced in the nonlinear theory by a velocity- and roughness-dependent parameter λ_α that plays a similar role. Detailed results are given for three special types of $\zeta(h, k)$: (1) white roughness ($|\zeta|$ constant); (2) truncated white roughness ($|\zeta|$ constant for all wavelengths above a certain lower limit); (3) a single wavelength; and (4) cross-corrugated sinusoidal waves. The results are tested against field observations of sliding. Given sliding velocity v, basal shear stress τ, and rheological parameters, the theory predicts roughness values ζ for the different types of $\zeta(h, k)$. When compared with ζ values inferred from observed bedrock outcrops, predicted values for white roughness are somewhat too small, whereas for white roughness truncated at 3.53 meters, they are of the expected size ($\zeta \sim 0.05$). Predicted λ_α values range from 3 to 112 cm; high v (>20 m yr^{-1}) generally gives λ_α in the range 10–40 cm, and low v (<6 m yr^{-1}) 30–70 cm. The predicted thickness of the regelation layer (1–10 mm) agrees with observation, but the predicted λ_α values appear to be somewhat too small. Extensive separation of the ice sole from bedrock, due to tensile stresses set up in sliding, is predicted in icefalls, whereas for valley glaciers little separation is predicted, unless meltwater under a head of pressure comparable to half the glacier thickness has access to the bed. Extensive separation is not needed to account for typical sliding velocities, provided that the roughness spectrum is truncated. Observed features of glaciated bedrock indicate truncation, which results from glacial abrasion. For the truncated spectrum, the predicted dependence of v on τ is much more highly nonlinear than for the full white spectrum; this implies a relatively high sensitivity of sliding velocity to changes in glacier thickness or surface slope.

1. INTRODUCTION

About half the observed motion of temperate glaciers is ordinarily caused by a sliding of the ice mass as a whole over the bedrock beneath it, called basal sliding or slip [*Sharp*, 1954]. Basal sliding is probably responsible for the time-variation of glacier flow velocities over the year, for fluctuations in total glacier motion from year to year, and also for the greatly increased motions that occur during glacier surges [*Meier and Post*, 1969]. For all these reasons, a quantita-

tive understanding of the basal sliding phenomenon is essential to any complete theory of glacier flow, and to any detailed discussion of the relationship between glacier fluctuations and climatic change [*Nye*, 1963]. The basal sliding phenomenon is also of interest in the wider context of tectonics, because certain tectonic events, such as the implacement of nappes or thrust sheets, involve a similar velocity discontinuity between a moving, glacier-like mass and a fixed substratum.

The physical requirements for basal sliding in glaciers were discussed by *Weertman* [1957], who formulated a theory of glacier sliding based on a simple model of the glacier bed, consisting of cubical or rectangular bedrock obstacles rising from a plane. *Kamb and LaChapelle* [1964] first observed the actual sliding process in such a way as to compare it with theoretical ideas. They found that the basic qualitative features of the sliding mechanism discussed by *Weertman* [1957] could be confirmed, but that the theory did not conform quantitatively to observation (this point is reconsidered in section 17 of the present paper). It seemed possible that the quantitative failure of the theory might be due to the fact that the bedrock model used is a poor approximation to the actual shape of glaciated bedrock surfaces observed in nature, and also that the model has features that make an exact analysis difficult. These observations motivated the theoretical development presented here, some results of which were quoted by *Kamb and LaChapelle* [1964].

Although the presentation given is self-contained, there are substantial relationships both with Weertman's original treatment and with other theoretical developments published subsequently:

1. The recently published treatment of *Nye* [1969] is similar to sections 5–8 in basic approach, and, where results can be compared, they agree exactly. Sections 5–8 contain an essentially exact analysis of the sliding of a linearly viscous body over general bedrock topography of low roughness. The present compact treatment emphasizes the Fourier-analytical approach, to the exclusion of other points of view considered by Nye, and it is built around the concept of the roughness spectral function $\zeta(h, k)$ introduced in section 4, a feature absent from Nye's development.

2. The approximate theory of sliding for a nonlinearly viscous material, developed in sections 10–13 from the linear theory in sections 5–9 as a starting point, is entirely new, but it bears some relationships with previously published treatments. Both the theories of *Weertman* [1957, 1964] and *Lliboutry* [1959, 1965, 1968] take the nonlinear rheology of ice into account; they differ from the present treatment in being more intuitively constructed and in not reducing to an essentially exact treatment for linear rheology. The bedrock model used in Weertman's theory is quite unlike actual glaciated bedrock topography, hence the roughness parameters of the theory cannot be directly related to actual field examples. In Lliboutry's theory, a more realistic bedrock topography, consisting of sinusoidal waves, is considered, but the Fourier-analytical method is not introduced, and arbitrary bedrock topography is not handled. In spite of the differences mentioned, many of the results obtained in these earlier treatments have a general similarity to the results of the present approach in sections 10–13. In particular, the type of nonlinearity in the dependence of basal shear stress on sliding velocity turns out to be the same in Weertman's theory and in the present theory, if comparable assumptions as to the roughness spectrum are made. (Lliboutry's theories give a quite different dependence.) The numerical factors appearing in the results of the different theories are, however, different, and the dependence on roughness is different in detail. None of the previous theories consider the detailed differences in results to be expected for different types of roughness spectra, and none consider the particular significance of what is here termed the truncated white roughness spectrum.

3. In sections 14–19, the theoretical results of sections 10–13 are applied to a group of well-studied field examples of glacier sliding, so as to test the theory quantitatively. Many of the subjects considered have been discussed from various points of view in the papers cited above; the present discussion is more systematic and comprehensive, and more closely tied to a variety of pertinent field observations. The size of the transition wavelength and thickness of the regelation layer (sections 17 and 18) are considered by *Nye* [1969, 1970] on the basis of the linear theory, and the results are generally similar though less detailed. The separation of ice from bedrock (section 19) is a feature of the sliding process strongly emphasized by *Lliboutry* [1959, 1965, 1968], and discussed also, with considerable difference of opinion, by *Weertman* [1964, 1967]. The approach in section 19 is intermediate between the points of view advocated by Weertman and Lliboutry.

The nonlinear sliding theory in sections 10–13 is an approximation developed by using the linear theory in sections 5–9 as a guide to important features of the nonlinear problem; it carries the nonlinear theory to about as good a degree of approximation as can be reached in a simple way, while retaining the basic advantages and attractiveness of a development based on Fourier analysis of the bedrock topography. Although further refinements are possible, the results even at this stage of approximation are sufficiently complex that one wishes to know whether they provide a reasonable quantitative description of the sliding process in nature. The tests in sections 14–21 indicate that in a general way they do. The limitations on agreement between theory and observation are probably as much a reflection of the insufficiency of pertinent and adequately detailed field observations and measurements as they are of inadequacies in the theory. I hope that the discussion given will serve as a spur to acquisition of the needed measurements and observations on glaciers.

2. SYNOPSIS OF SYMBOLS

A Area of arbitrary part of bedrock topography for which the relation between v and τ is calculated (equation 3).

A' $= L_1 L_2$.

a Amplitude of single topographic sinusoidal wave, or of cross-corrugated sinusoid (93), (98).

$a(h, k)$ Amplitude function in Fourier integral representation of bedrock topography (3).

a_{mn} Coefficients in Fourier-series representation of bedrock surface (1).

a_P Amplitude of sliding adjustment to bed topography by plastic flow, for Fourier component h, k (34), (38).

a_R Amplitude of sliding adjustment to bed topography by regelation, for Fourier component h, k (34), (37).

$B(h, k)$ Amplitude function in Fourier integral representation of temperature distribution (10).

C Constant in flow solution for velocity field for a single Fourier component (24).

$C(h, k)$ Same as C, with wavelength dependence indicated (27).

C_0 Coefficient in melting-point lowering of ice under pressure (18).

$\bar{d}_R$ Estimate of mean thickness of the regelation layer (112)–(115).

$\dot{e}_{ij}$ Strain-rate tensor components (23).

f 'Channel-shape factor' for calculating τ (97).

g Gravitational acceleration.

$g(\mu)$ Function giving dependence of τ contribution on wavelength (108).

$G(\zeta; n)$ Function containing effect of nonconstant $\mathfrak{L}(l)$ on τ for white roughness (77), Figure 4.

H Latent heat of ice per unit volume (8).

h, k Wave-vector components of the sinusoidal waves in the Fourier integral representation of the glacier bed (3).

h_I Thickness of glacier ice, measured vertically (97), (119).

h_W Height of water level above bed, measured vertically (120).

K_1, K_2 Thermal conductivity of ice, bedrock (9).

l $= (h^2 + k^2)^{1/2} = 2\pi/\lambda$. Wave-vector amplitude (or wave number) (5).

l_0 Transition wave number for linear theory (36).

l_L Wave-number limit for truncated white roughness spectrum (80).

l_α Effective transition wave number in nonlinear theory (69), (80), (91). Also, wave-number parameter for nondimensionalizing (65).

$\mathfrak{L}(l)$ Wavelength-dependent quantity corresponding to l_0, for nonlinear flow (62).

L_1, L_2 Dimensions of a rectangular part of the bedrock topographic surface (1).

$M(\zeta; n)$ Function containing effect of nonconstant $\mathfrak{L}$ on τ for truncated white roughness (89), Figure 5.

N Constant in nonlinear viscosity formula (58).

n Exponent in nonlinear dependence of strain rate on stress (59).

$p(x, y, z)$ Mean pressure in flowing fluid (19).

$P_0(x, y)$ Pressure in water film at ice-rock interface, minus the constant pressure σ; normal pressure (minus σ) at base of ice (18), (30).

$\langle P_0^2 \rangle$ Mean square of the pressure fluctuations at base of ice, averaged over area A (116).

P_W Pressure of water in passageways having access to the bed (120).

$q(x, y)$ Heat flux arriving at the ice-bedrock interface (8).

$Q(h, k)$ Fourier transform of $q(x, y)$ (12).

R Numerical correction factor for relation between velocity and stress at base of ice (60).

s 'Smoothness ratio' in theory of *Weertman* [1964, 1969], section 17.

$T_1(x, y, z)$ Temperature distribution in ice ($z \gtrsim 0$) (10).

$T_2(x, y, z)$ Temperature distribution in bedrock ($z \lesssim 0$) (11).

$T_0(x, y)$ Temperature at the ice-bedrock interface; approximated by $T_1(x, y, 0)$ (17).

$\mathbf{u}$ Flow velocity vector (19).

u_x, u_y, u_z Components of $\mathbf{u}$ (22).

v Sliding velocity (32), Figure 1.

v_P Sliding velocity if only plastic flow operated (21).

v_R Sliding velocity if only regelation operated (8).

$V(\mu, \zeta)$ Nondimensionalized reciprocal viscosity function for truncated white roughness (84).

$X(\mu, \zeta)$ Nondimensionalized reciprocal viscosity function for white roughness (73).

x, y Space coordinates; the x, y plane is a least-squares fit to the bedrock topography over area A, and x is in the direction of the sliding motion (1).

z Space coordinate measured normal to the x, y plane, increasing into the ice (9).

$z_0(x, y)$ Equation of bedrock topographic surface (1), Figure 1.

$z_R(x, y)$ Contribution of regelation to bedrock accommodation in sliding (110).

$Z(\mu_x, \mu_y)$ Normalized roughness spectral function (65).

α $= 1 - 1/n$. Exponent in nonlinear viscosity formula (58).

β Local slope of bed in x direction, measured relative to the x, y plane (102).

β_{max} Maximum upglacier value of β (102).

β_m Estimate of maximum upglacier value of β for arbitrary topography (105).

β_m' β_m based on an average over a limited wavelength spectral range, section 16.

Γ $= H/[2C_0(K_1 + K_2)]$. Constant used in nonlinear theory (62).

$\dot{\epsilon}$ Second strain-rate tensor invariant (48).

$\langle \dot{\epsilon}^2(z) \rangle$ Average of $\dot{\epsilon}^2$ over the area A, at a given height z (51), (57).

$\dot{\epsilon}_{max}$ Maximum value of $\langle \dot{\epsilon}^2(z) \rangle^{1/2}$, for given sliding conditions, Table 6, section 20.

ζ Roughness value for white roughness (7), or for a single wavelength (93).

$\zeta(h, k)$ Roughness spectral function (5).

$\zeta(l)$ Roughness spectral function for isotropic topography (44).

ζ_0 Normalizing constant for roughness spectrum (65).

η Viscosity coefficient (19), (58).

$\eta(z)$ z-dependent viscosity coefficient, for nonlinear flow (60).

θ Slope of glacier surface (97).

$\Theta(p)$ Function giving z dependence of η for truncated white roughness (85).

$\Theta(1)$ $= 8.14 \times 10^{-3}$. Value of $\Theta(p)$ at $p = 1$ (84).

κ = P_w/σ. Ratio of water pressure to ice overburden pressure at glacier bed (72).
κ_i Thermal diffusivity of ice (10).
λ = $2\pi/l$. Wavelength of a sinusoidal wave (5).
λ_0 = $2\pi/l_0$. Transition wavelength for linear theory (36), section 17.
λ_α = $2\pi/l_\alpha$. Effective transition wavelength in nonlinear theory (69), section 17.
λ_1, λ_2 Lower and upper wavelength limits used in calculating β_m (105).
λ_L = $2\pi/l_L$ Truncation wavelength (lower wavelength limit for truncated white roughness spectrum) (80).
μ, μ_x, μ_y Nondimensional wave number components (65).
Λ 'Controlling obstacle size' of *Weertman* [1964] (109*a*).
Λ' Lower limit of effective obstacle sizes in theory of *Weertman* [1964], section 12.
$\Xi(p)$ Function giving z dependence of ϵ for sliding in white roughness (52).
ξ = $l_\alpha z$. Nondimensionalized z coordinate (65).
$\Pi(h, k)$ Fourier transform of $P_0(x, y)$ (31).
Π_R, Π_P $\Pi(h, k)$ as required for regelation, plastic-flow sliding (32), (33).
ρ_w, ρ_I Density of water, ice (97), (120).
σ Pressure contribution due to weight of ice overburden, at base of glacier (119).
τ Basal shear stress (drag stress due to sliding), averaged over area A (40).
τ_{ij} Stress tensor components (23).
$\varphi(\xi)$ Normalized reciprocal viscosity function (66).
$\Omega(p)$ = $(3/2\pi^4)(\Xi(p))^2$ (71).
$\Omega(2)$ = 2.68×10^{-2}. Value of $\Omega(p)$ at $p = 2$ (72).
$\langle\ \rangle$ Average over coordinates x, y (4).

3. PHYSICAL MODEL AND OUTLINE OF ANALYSIS

Ice at the melting point overlies a bedrock surface $z = z_0(x, y)$, where z_0 is the height z of the surface above a reference plane (the x, y plane) taken as a best over-all fit to the bedrock topography over the area of interest. The ice is moving with an over-all velocity v, the sliding velocity, in the $+x$ direction. Sliding is possible because the ice is not frozen to the bedrock, a thin layer of water (a few microns thick) intervening between ice and bedrock. The ice-bedrock interface is accordingly shear-stress free, and the resistance to sliding is caused by the bedrock irregularities that obstruct the motion.

Sliding of the ice past the irregularities takes place by two processes. (1) On the upstream faces of bedrock irregularities, where there is increased normal pressure across the ice-bedrock interface, the local melting temperature is lowered; heat is conducted to these areas, and melting occurs there, allowing the ice to move forward; the meltwater migrates along the ice-rock interface and refreezes on the downstream faces, where the normal pressure is reduced and the melting temperature raised; the heat released on freezing here is the source of the heat conducted to the upstream faces and is in turn required there for

melting. This process of melting and refreezing is here called 'regelation,' and its contribution to the sliding process is called 'regelation sliding' (the use of the term 'regelation' in this context is discussed by *Kamb and LaChapelle* [1964, p. 160]). (2) The ice responds plastically to the increased normal pressure on the upstream faces, arching upward at these points and thereby permitting the ice to move forward; correspondingly, it closes down behind the irregularities, in response to the reduced normal pressure on the downstream faces. The sliding contribution of this process is called 'plastic-flow sliding.' The plastic-flow response of the ice is assumed to be that of a generalized Newtonian fluid, rather than plasticity in the strict sense.

The sliding process defined by these specifications is illustrated schematically in Figure 1. We seek a relationship between the sliding velocity v and the drag

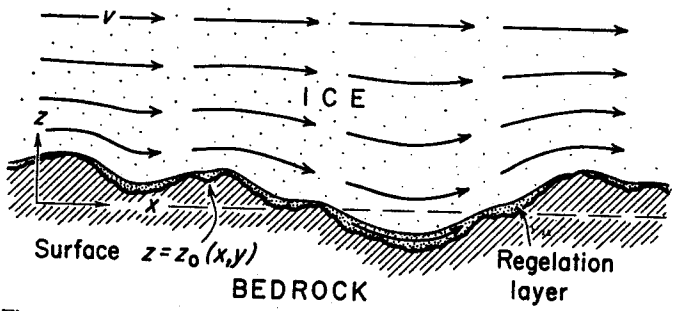

Fig. 1*a*. Schematic representation of ice sliding with velocity v over an arbitrary bedrock topographic surface $z = z_0(x, y)$. Coordinate system is as shown, with the x axis in the sliding direction. A cross section of the bed in the y direction (perpendicular to the direction of sliding) would be generally similar to the x cross section shown. The regelation layer consists of ice formed by the refreezing of water that has migrated along the ice-rock contact from areas of high normal pressure. Warping of the ice flow vectors near the bedrock surface is an indication of plastic deformation taking place in the ice.

stress or basal shear stress τ, as a function of bed roughness, appropriately defined. For this purpose the bedrock topography $z_0(x, y)$ is Fourier analyzed, and the regelation and plastic-flow contributions to the sliding motion are calculated separately for the individual Fourier components. This analysis can be carried out rigorously when the amplitudes of the Fourier components are small compared to their wavelengths, that is, when the roughness is low enough that the heat and plastic-flow problems can be treated as problems in a half-space. For the plastic-flow problem, a rigorous analysis is possible in the case of linear rheology (Newtonian viscosity), and a practical approximation to nonlinearity can be developed from this as a starting point. The results can then be appropriately combined to obtain τ as a function of v for sliding under the simultaneous operation of regelation and plastic flow. In making this combination, there emerges a characteristic length λ_α, here called the transition

wavelength, that governs the relative contributions of regelation and plastic flow to the sliding process. It is the fundamental parameter of the theory, and can be tested against field observations, as can other theoretically derivable quantities such as the thickness of the regelation layer, i.e., the ice layer involved in the regelation process as shown in Figure 1.

4. DESCRIPTION OF BEDROCK TOPOGRAPHY AND ROUGHNESS

To analyze the relation between sliding velocity v and basal shear stress τ, we consider a part of the bed of area A' over which v is essentially constant. Within this area, assumed to be rectangular of dimensions L_1 and L_2 in the x and y directions, we Fourier analyze the bedrock topography:

$$z_0(x, y) = \sum_{m=-\infty}^{+\infty} \sum_{n} a_{mn} \exp\left[2\pi i\left(\frac{mx}{L_1} + \frac{ny}{L_2}\right)\right] \tag{1}$$

Here and in all such equations to follow, involving a real quantity on the left side and (in general) a complex quantity on the right side, it is understood that the real part of the complex quantity is meant. To calculate the relation between τ and v over the area A', we can suppose the topography described by (1) to be continued over the entire x, y plane, so that the bed, of assumed infinite extent, consists of a checkerboard of identical areas A', across which the ice slides with constant velocity v in the x direction.

The appropriate size of the area $A'(=L_1L_2)$ is constrained by the assumption that v is essentially constant over this area. The nature of this constraint will be examined in a separate paper; it will be shown that the appropriate distances L_1 and L_2 must be ~100 meters. Since real topography is not periodic, there is nothing in real topography to correspond to the arbitrary repeat distances L_1 and L_2 or the discrete spectrum of wave amplitudes a_{mn} in (1). It is therefore conceptually better to replace this discrete spectrum with a continuous spectrum $a(h, k)$, in which the wave vector components h and k are continuous and are related to m and n by making the replacements

$$(2\pi/L_1)m \to h \qquad (2\pi/L_2)n \to k$$
$$a_{mn} \to a(h, k) \tag{2}$$

This modification can be made if we write (1) in the form

$$z_0(x, y) = \sum_{m=-\infty}^{+\infty} \sum_{n} a_{mn} \exp\left[2\pi i\left(\frac{mx}{L_1} + \frac{ny}{L_2}\right) \Delta m\, \Delta n\right]$$

(where Δm and Δn are, of course, 1), and then use (2) to convert this to

$$z_0(x, y) = \frac{A'}{4\pi^2} \sum_{h=-\infty}^{+\infty} \sum_{k} a(h, k) \exp i(hx + ky)\, \Delta h\, \Delta k$$

If we now let A' become very large, the right side of this equation tends to an integral:

$$z_0(x, y) = \frac{A}{4\pi^2} \iint_{-\infty}^{+\infty} a(h, k) e^{i(hx+ky)}\, dh\, dk \tag{3}$$

Strictly speaking, the Fourier integral in (3) cannot be written unless the convergence requirement (existence of $\iint_{-\infty}^{+\infty} |z_0(x, y)|\, dx\, dy$) is satisfied, and this requires that we give up the continuation, over the full x, y plane, of topography with typical nonzero amplitude z_0. For this reason A' has been replaced by A in (3); we take A to be an area that is finite but very large, much larger than any area of practical interest, and we suppose that the topographic amplitude z_0 shows normal characteristics within area A and is zero outside A. In calculating the average drag stress τ produced by sliding of the ice mass at constant velocity v across the area A, we will simply compute the total resisting drag force, and divide by the area A. Although there will be unwanted edge effects owing to the termination of nonzero z_0 at the boundary of A, these effects become negligible when A is very large, because the contribution of the edge effects to the drag goes as $A^{1/2}$, whereas the main contribution goes as A.

In spite of the conceptual difference between the A' in (1) and the A in (3), the results of sliding theories developed on the basis of (1) and (3) turn out to be identical, in the sense that all the pertinent sums over the discrete spectrum correspond to integrals over the continuous spectrum according to the relationship

$$\sum_{m,n=-\infty}^{+\infty} \to \frac{A}{4\pi^2} \iint_{h,k=-\infty}^{+\infty} dh\, dk \tag{2'}$$

with $L_1L_2 \to A$ in (2'). Because the continuous spectrum is conceptually better, we will use (3) as the starting point for developing the theory here. In application of the theory to an actual field example of bedrock topography, however, it will be necessary to Fourier analyze the topography over a finite area. Then the results of the theory given here can be utilized by converting them to a discrete spectrum by means of the correspondences in (2) and (2'). Because L_1 and L_2 must be large compared to topographic wavelengths that have a significant effect on the relation between τ and v, the practical difference between the two approaches, based on (1) and (3), is negligible.

The bed roughness, which enters as an important parameter into the relation between τ and v for sliding, can be defined in terms of $\langle z_0^2 \rangle$, the mean-square topographic amplitude averaged over the area A. Since we choose the x, y plane to be a best fit to the topography in a least-squares sense, $\langle z_0^2 \rangle$ is a measure of the 'strength' of the topographic fluctuations. From the previously stated restriction of nonzero $z_0(x, y)$ to the interior of area A, it follows that

$$\langle z_0^2 \rangle \equiv \frac{1}{A} \iint_{A} z_0^2(x, y)\, dx\, dy = \frac{1}{A} \iint_{-\infty}^{+\infty} z_0^2\, dx\, dy$$

and hence, by standard Fourier theory,

$$\langle z_0^2 \rangle = \frac{A}{4\pi^2} \iint_{-\infty}^{+\infty} a^2(h, k)\, dh\, dk \tag{4}$$

where a^2 is written for $|a|^2$.

It is found that the sliding process depends not so much on the over-all measure of roughness (4) as on the distribution of roughness over the wavelength spectrum. The spectral distribution of roughness is best defined in terms of the contributions of different wavelengths to $\langle z_0^2 \rangle$. It is intuitively advantageous to use as a nondimensional measure of the roughness at a given wavelength the ratio ζ of wave amplitude to wavelength. To treat the contributions at different wavelengths on a uniform basis, we designate by $(\zeta\lambda)^2 \cdot (dh/l)\,(dk/l) \cdot (3\pi)^{-1}$ the contribution to $\langle z_0^2 \rangle$ of the topographic 'strength' within logarithmic wavenumber intervals dh/l and dk/l. Here l is the wave vector amplitude $l = (h^2 + k^2)^{1/2}$, and the wavelength is $\lambda = 2\pi/l$. The roughness spectral function $\zeta(h, k)$ defined in this way can be related to $a(h, k)$ by equating the corresponding contributions to $\langle z_0^2 \rangle$:

$$\frac{A}{4\pi^2}\, a^2(h, k)\, dh\, dk = (\zeta(h, k)\lambda)^2 \cdot \frac{dh\,dk}{l\ l} \cdot \frac{1}{3\pi} \tag{5}$$

Since $\lambda = 2\pi/l$, (5) gives the following definition of $\zeta(h, k)$:

$$\zeta(h, k) \equiv A^{1/2} \frac{3^{1/2}}{4\pi^{3/2}}\, l^2 a(h, k) \tag{6}$$

The arbitrary factor $1/3\pi$ in (5) is introduced so that, if $\zeta(h, k)$ is constant, independent of wavelength, the contribution to $\langle z_0^2 \rangle$ over one octave of wavelength (from $l = l_1/2^{1/2}$ to $l = l_1 2^{1/2}$, where l_1 is arbitrary) is equal to $\frac{1}{2}\zeta^2\lambda_1^2$, i.e., just that of a sine wave of amplitude $\zeta\lambda_1$:

$$\frac{A}{4\pi^2} \iint_{l=l_1/2^{1/2}}^{l=l_1 2^{1/2}} a^2(h, k)\, dh\, dk = \frac{4}{3}\pi \int_{l_1/2^{1/2}}^{l_1 2^{1/2}} \frac{\zeta^2}{l^4}\, 2\pi l\, dl = \frac{1}{2}\zeta^2\lambda_1^2 \tag{7}$$

The analytical results are best stated in terms of the roughness spectral function $\zeta(h, k)$, rather than in terms of $a(h, k)$. The situation $|\zeta(h, k)| = \zeta =$ constant will be called the case of a white roughness spectrum with roughness parameter ζ. Physically it represents the situation in which, at all wavelengths, the amplitudes of the topographic waves present are a constant fraction ζ of the wavelengths. The significance of departures from the white spectrum is easily visualized against this as a standard.

If for a white roughness spectrum we blindly compute, from (4),

$$\langle z_0^2 \rangle = \frac{4\pi^2}{3}\zeta^2 \int_0^\infty \frac{dl}{l^3}$$

we see that the resulting integral is divergent at the lower limit. This corresponds to the increasingly large contributions from the increasingly long waves, and it violates the convergence requirement for the Fourier integral in (3). The difficulty can be avoided by terminating the white spectrum at some very long but finite wavelength λ_2. Strictly speaking, the suppression of $z_0(x, y)$ outside the area A imposes a constraint on the form of the function $\zeta(h, k)$ that cannot necessarily be satisfied simply by terminating the white roughness spectrum abruptly at any arbitrary λ_2, but that does require suppression of wave amplitudes for $\lambda \gtrsim A^{1/2}$. We shall not consider here the detailed nature of this constraint, because the results of the sliding theory (section 8) turn out to be insensitive to $\zeta(h, k)$ for $\lambda \gg \lambda_0 \sim 1$ meter, and because we know from the standard theory of wave packets that the suppression of z_0 outside area A will have very little effect on the spectrum $\zeta(h, k)$ for wavelengths $\lambda \sim \lambda_0 \ll A^{1/2}$.

5. REGELATION SLIDING

When sliding occurs by the regelation mechanism alone, the ice moves forward as a rigid mass with velocity v_R in the x direction. If the ice is everywhere in contact with its bed, and if there is no net loss or addition of material as the ice slides, then the movement requires ice to melt or refreeze at the ice-bedrock interface at a rate $v_R \partial z_0/\partial x$, expressed in volume of ice per unit area of the x, y plane per unit time, hence requiring heat to be delivered to this interface at a rate

$$q(x, y) = H v_R\, \partial z_0/\partial x \tag{8}$$

per unit area in the xy plane. H is the latent heat per unit volume of ice. Where $q(x, y)$ in (8) is positive, the interface acts as a heat sink, and where negative, a heat source. For sliding to take place by regelation, the temperature distribution in the ice and bedrock must adjust itself so that the necessary heat flux (8) is delivered to the interface.

We assume that the heat transport is accomplished purely by thermal conduction in the temperature field so established, since it can be shown that the advective heat transport in the water layer is negligible. We also assume that the water layer itself presents a negligible thermal barrier, since the layer is very thin in comparison with the conduction distance scale of decimeters that is pertinent to the sliding process in practice, as will be shown. Studies of regelation of wires moving through ice [*Nye*, 1967] show that the thermal resistance of the water layer is important only for very thin wires and hence for very short conduction paths in the solids.

We therefore seek the temperature distribution $T_0(x, y)$ on the interface $z = z_0(x, y)$ such that the flux of heat $q(x, y)$ given by (8) will be delivered to the interface by thermal conduction through the ice above (conductivity K_1) and the bedrock below (assumed homogeneous, of conductivity K_2). This problem is readily solved if the surface $z_0(x, y)$, as viewed at pertinent roughness wavelengths, is nearly enough planar that the heat flows in the ice and the bedrock can be treated as flows in a half-space. This requires the roughness $\zeta(h, k)$ to be small over the pertinent wavelengths (wavelengths less than several meters, as shown in section 17). It also requires the ice thickness to be much greater than the pertinent wavelengths. Although the quantitative limitations on the accuracy of the analysis based on these assumptions will not be investigated here, it is clear that the effects of nonplanarity of the interface will tend to

be compensated to first order by the heat conduction on the two sides of the interface, since the conduction paths on one side of the interface lengthen as those on the other side shorten, and since $K_1 \approx K_2$ for most rocks.

On this basis we solve the heat-flow problems in the half spaces above and below the x, y plane, with the boundary condition for $q(x, y)$ in (8) given on the x, y plane rather than on the actual surface $z_0(x, y)$. We suppose that a steady state has been reached, so that in the lower half-space the temperature $T_2(x, y, z)$ satisfies

$$\nabla^2 T_2 = 0$$

and in the upper half space $T_1(x, y, z)$ satisfies

$$\kappa_1 \nabla^2 T_1 = v_R \, \partial T_1 / \partial x$$

where $\kappa_1 = K_1/c_1$ is the thermal diffusivity of ice. These equations are to be solved subject to the boundary conditions $T_1 = T_2$ and

$$K_1 \frac{\partial T_1}{\partial z} - K_2 \frac{\partial T_2}{\partial z} = q(x, y) \tag{9}$$

at $z = 0$, and the conditions $T_1 \to 0$ as $z \to \infty$ and $T_2 \to 0$ as $z \to -\infty$. The solutions are conveniently represented in terms of Fourier components as follows:

$$T_1 = \frac{A}{4\pi^2} \iint B(h, k) \exp\left[-lz\left(1 - \frac{v_R}{\kappa_1} \frac{h}{l^2} i\right)^{1/2}\right] \cdot e^{i(hx+ky)} \, dh \, dk \tag{10}$$

$$T_2 = \frac{A}{4\pi^2} \iint B(h, k) \exp(lz) \cdot e^{i(hx+ky)} \, dh \, dk \tag{11}$$

Letting $Q(h, k)$ represent the Fourier components of q, so that

$$q(x, y) = \frac{A}{4\pi^2} \iint Q(h, k) e^{i(hx+ky)} \, dh \, dk \tag{12}$$

then the function $B(h, k)$ is determined in relation to $Q(h, k)$ by (9)

$$-\left[K_1 l\left(1 - \frac{v_R}{\kappa_1} \frac{h}{l^2} i\right)^{1/2} + K_2 l\right] B(h, k) = Q(h, k) \tag{13}$$

For $v_R h/\kappa_1 l^2$ sufficiently small, (13) is approximately

$$-B(K_1 + K_2)\left(1 - \frac{K_1}{K_1 + K_2} \frac{v_R}{\kappa_1} \frac{h}{l^2} i\right) = Q \tag{14}$$

For $v_R = 20$ m yr^{-1} and $\lambda = 2\pi/l = 2$ meters, the imaginary part of the last factor on the left in (14) is approximately $-0.1i$. This contributes a phase shift of about 6° between the Fourier components of flux and temperature, which would otherwise be exactly out of phase; it also affects the magnitude of B (in relation to Q) by about 0.5%. These effects are too small to merit inclusion here, and they become smaller for smaller wavelengths, so that they are negligible for all wavelengths at which regelation contributes significantly to the sliding mechanism in practice. Hence in (10) and (13) the imaginary term $v_R h i/\kappa_1 l^2$ can be dropped, which corresponds to neglecting the advective transport of heat by the moving ice. We thus get

$$B(h, k) = -Q(h, k)/l(K_1 + K_2) \tag{15}$$

$Q(h, k)$ is determined from (8), (3), and (12) as

$$Q(h, k) = H v_R i h a(h, k) \tag{16}$$

The temperature distribution at the ice-rock interface is then given by

$$T_0(x, y) = \frac{A}{4\pi^2} \iint B(h, k) e^{i(hx+ky)} \, dh \, dk \tag{17}$$

with $B(h, k)$ from (15) and (16).

The temperature distribution (17) is linked to the pressure $P_0(x, y)$ in the water film between ice and bedrock by the requirement that the ice be at its melting point at the interface. Although the ice may in general be nonhydrostatically stressed, thermodynamic theory [*Kamb*, 1961, 1963] shows that, for ice in equilibrium with water at pressure P, the temperature at the water-ice interface is to first order the same as though the ice were hydrostatically stressed at pressure P, and the higher-order correction terms are negligible for stresses that occur in glacier ice. Hence the pressure $P_0(x, y)$ across the ice-rock interface, which is also the pressure in the thin water layer, is related to the temperature there by the simple linear relation

$$T_0(x, y) = -C_0 P_0(x, y) \tag{18}$$

where $C_0 = 0.0074$°C bar^{-1}.

6. PLASTIC-FLOW SLIDING FOR LINEAR RHEOLOGY

If regelation did not operate but the ice-rock interface remained lubricated, the ice mass could move forward with an over-all velocity v_P, provided that vertical motions of the ice adjacent to the bed allowed a continually adjusting accommodation of the ice to the bedrock irregularities. The problem is to determine what distribution of pressure $P_0(x, y)$ on the interface will produce the required vertical motions in the ice above. We examine first the relatively straightforward case in which the rheological behavior of the ice is assumed to be linear (Newtonian viscosity).

The problem is formulated as follows. For a Newtonian fluid flowing at velocities slow enough that inertial effects can be neglected, the velocity field $\mathbf{u}(x, y, z)$ satisfies

$$\eta \nabla^2 \mathbf{u} - \nabla p = 0 \tag{19}$$

where $p(x, y, z)$ is the mean pressure ($p = -\frac{1}{3}\tau_{kk}$, where the τ_{ij} are the stress-tensor components), and η is the viscosity coefficient. The flow is incompressible, so that

$$\nabla \cdot \mathbf{u} = 0 \tag{20}$$

Equations 19 and 20 are to be solved subject to the condition $\mathbf{u} \to v_P \mathbf{e}_x$ as $z \to \infty$, and on the surface $z = z_0(x, y)$, the conditions (a) that $\mathbf{u}$ be tangential to the surface, and (b) that the shear stress parallel to the surface vanish. Condition (b) follows from the lubrication of the ice-rock interface by the water layer; it

can be shown that the shear stress supported by this layer, in spite of its small thickness, is negligible.

Condition (a) can be specified to an adequate degree of approximation by assuming that $u_x = v_P$ and $u_y = 0$ at the interface $z = z_0(x, y)$; this assumption becomes strictly true as the roughness tends to zero. If the ice conforms to its bed everywhere, the required motions in the z direction at the boundary $z = z_0(x, y)$ are then

$$u_z = v_P \, \partial z_0/\partial x \tag{21}$$

We do not constrain u_x on the interface boundary $z = z_0$, but instead show that the condition for this boundary to be free of shear stress leads to the result $u_x = v_P$, consistent with the assumption used in deriving (21).

A solution of (19) and (20) that satisfies the boundary conditions stated can be readily given if the roughness is low enough that the viscous flow can be assumed to take place effectively in a half-space, and the interface boundary conditions are therefore applied at $z = 0$ rather than at $z = z_0(x, y)$. Under this assumed to take place effectively in a half-space, and the interface boundary conditions $\tau_{xz} = \tau_{yz} = 0$, all at $z = 0$. To first order in the slope $\partial z_0/\partial x$ of the interface, the normal stress τ_{zz} across the x, y plane will be the same as the normal stress $\tau_{z'z'}$ across the tilted plane parallel to the interface, so that we can associate $P_0(x, y)$ directly with $-\tau_{zz}(x, y, 0)$ from the flow solution. To first order there will, however, be a nonzero τ_{xy} across the x, y plane, consistent with the fact that $\langle \tau_{xy} \rangle = \tau \neq 0$. We omit this nonzero τ_{xy} from the flow solution for the following reason. Consider the flow problem for a single Fourier component of the bedrock topography. The nonzero, fluctuating τ_{xy} acting parallel to the x, y plane is applied at a wavelength half that of the appropriate Fourier component of $u_z(x, y)$ or $P_0(x, y)$. It leads to velocities $u'_x(x, y, 0)$ that are second order in a_{hk}/λ, relative to the driving velocity v_P, and that oscillate with wavelength $\lambda/2$. If we were to incorporate these velocities into the solution, we would affect the boundary condition (21) and thereby introduce a coupling between motions at wavelength λ, $\lambda/2$, $\lambda/4$, $\cdots$, destroying the simplicity of the linear solution in which the Fourier components are uncoupled. The second-order dependence of the resultant $u'_x(x, y, 0)$ on a_{hk}/λ allows these coupling effects to be neglected for low roughness, which is then equivalent to returning to the stress boundary condition $\tau_{xz} = \tau_{yz} = 0$. The stress and flow distribution above the undulating boundary $z_0 = a \sin hx$ has been investigated in detail by W. D. Harrison (unpublished data, 1969), and his results confirm the foregoing argument.

By standard methods, the following solution to (19) and (20) is readily derived:

$$\begin{aligned} u_x &= -\frac{1}{l^2}(hlC + kD - hE + hlEz)e^{-lz}ie^{i(hx+ky)} + v_P \\ u_y &= -\frac{1}{l^2}(klC - hD - kE + klEz)e^{-lz}ie^{i(hx+ky)} \\ u_z &= (C + Ez)e^{-lz}e^{i(hx+ky)} \end{aligned} \tag{22}$$

where C, D, and E are constants, and where $l = \pm(h^2 + k^2)^{1/2}$. Because of the condition at $z \to +\infty$, the positive root is taken. The stress boundary conditions at $z = 0$ are applied to (22) via the stress–strain rate equations

$$\tau_{ij} = 2\eta\dot{e}_{ij} - \delta_{ij}p \tag{23}$$

For the conditions $\tau_{xz} = \tau_{yz} = 0$, the pressure p does not enter, and the resulting conditions on the constants in (22) are $D = 0$ and $E = Cl$. The velocity solution (22) therefore simplifies to

$$\begin{aligned} u_x &= -Chze^{-lz}ie^{i(hx+ky)} + v_P \\ u_y &= -Ckze^{-lz}ie^{i(hx+ky)} \\ u_z &= C(1 + lz)e^{-lz}e^{i(hx+ky)} \end{aligned} \tag{24}$$

We see that $u_x(x, y, 0) = v_P$, and $u_y(x, y, 0) = 0$, as was assumed in the derivation of (21).

The boundary normal stress $\tau_{zz}(x, y, 0)$ given by (23) and (24) is simply $\tau_{zz} = -p(x, y, 0)$, since $\partial u_z/\partial z = 0$ at $z = 0$. The pressure p, which is required in a complete specification of the solution of (19) and (20), is derivable from (19) and (24), and is

$$p(x, y, z) = 2\eta Cle^{-lz}e^{i(hx+ky)}$$

so that at the boundary we have

$$\tau_{zz}^{(x,y,0)} = -2\eta Cle^{i(hx+ky)} \tag{25}$$

or simply

$$\tau_{zz} = -2\eta l u_z(x, y, 0) \tag{26}$$

The constant C is to be evaluated from (21). For general bedrock topography in the form (3), the velocity field and stress must be represented by Fourier integrals over the results in (24) and (25), with C taken to be a function of h and k:

$$u_z(x, y, 0) = \frac{A}{4\pi^2}\iint C(h, k)e^{i(hx+ky)}\,dh\,dk \tag{27}$$

$$\tau_{zz}(x, y, 0) = -\frac{A}{4\pi^2}\iint 2\eta lC(h, k)e^{i(hx+ky)}\,dh\,dk \tag{28}$$

where from (21) and (3)

$$C(h, k) = v_P hia(h, k) \tag{29}$$

The drag stress τ due to sliding will be calculated in section 8 from the stress distribution (28).

7. SLIDING BY SIMULTANEOUS REGELATION AND PLASTIC FLOW

It is necessary to take the two processes regelation and plastic flow in combination to get a physically possible mechanism of sliding, as was shown

originally by *Weertman* [1957]. If the roughness spectrum $\zeta(h, k)$ extends with nonzero roughness to very long wavelengths λ_2, then for fixed τ the sliding velocity v would tend to zero as $v\zeta^2/\lambda_2$ if regelation sliding alone operated; similarly, if the spectrum extends to very short wavelengths λ_1, then v would tend to zero as $v\zeta^2\lambda_1$ if plastic-flow sliding alone operated.

The combination of the regelation and plastic-flow contributions to sliding takes place with the constraint that both processes operate under the influence of the same pressure distribution across the ice-bedrock interface

$$\tau_{zz}(x, y, 0) = -P_0(x, y) \tag{30}$$

(An additive constant σ due to the weight of the ice overburden, whose importance is considered in section 19, has been omitted from $-\tau_{zz}(x, y, 0)$ as given by equation 28, and hence from $P_0(x, y)$ as given by equation 30.) The left-hand and right-hand sides of (30) are determined by (28) and (18). If we represent $P_0(x, y)$ in Fourier form,

$$P_0(x, y) = \frac{A}{4\pi^2} \iint \Pi(h, k) e^{i(hx+ky)}\, dh\, dk \tag{31}$$

then $\Pi(h, k)$ must be the same when calculated for regelation from (15)–(18) and for plastic flow from (28)–(30):

$$\Pi_R = \frac{H}{C(K_1 + K_2)} \frac{ih}{l} v a_R(h, k) \tag{32}$$

$$\Pi_P = 2\eta i h l v a_P(h, k) \tag{33}$$

In (32) we have written va_R in place of $v_R a$, and in (33) va_P in place of $v_P a$, for the following reason. The combination sliding mechanism can be thought of in two alternative ways: (*a*) the two sliding processes operate across topography of fixed amplitude a, and the resultant velocities v_R and v_P add to produce the actual sliding motion $v = v_R + v_P$; (*b*) both sliding processes operate at the actual sliding velocity v, but the amplitudes of vertical adjustment a_R and a_P produced by the two processes add to effect the complete accommodation of the ice to the actual bedrock topographic amplitude a. Since only the product va occurs in (16), (29), (32), and (33), the two views (*a*) and (*b*) are mathematically equivalent, but (*b*) is physically clearer and is adopted here. For topography consisting of a single Fourier component a, a_R is half the maximum thickness of the regelation layer and a_P is the half-amplitude of the sine wave defined by the top of the regelation layer (see Figure 1*b*).

For every Fourier component, we therefore have

$$a(h, k) = a_R(h, k) + a_P(h, k) \tag{34}$$

Setting $\Pi_R = \Pi_P$ in (32) and (33), we get

$$l_0^2 a_R(h, k) = l^2 a_P(h, k) \tag{35}$$

where

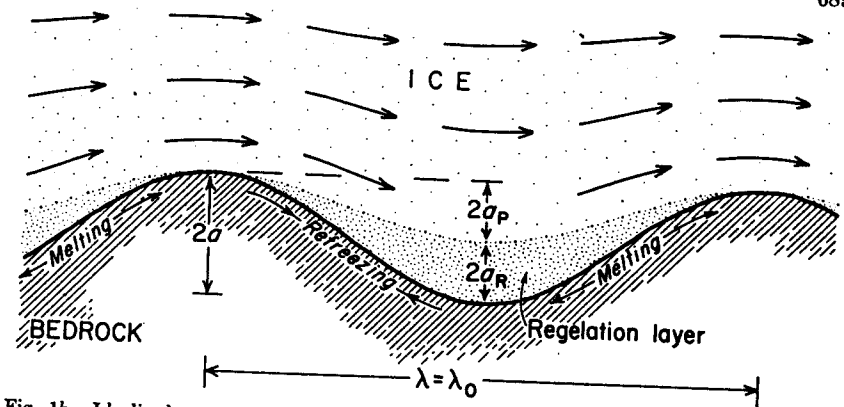

Fig. 1*b*. Idealized case of sliding across a bedrock surface of sinusoidal shape and wavelength λ equal to the transition wavelength λ_0. The amplitudes of adjustment by regelation, a_R, and by plastic flow, a_P, are equal in this case. Parts of the bedrock surface where melting and freezing of the regelation layer takes place are labeled.

$$l_0^2 \equiv \frac{H}{2\eta C_0(K_1 + K_2)} \tag{36}$$

The wavelength $\lambda_0 = 2\pi/l_0$ that arises in (35) and is given by (36) is the fundamental parameter of glacier sliding theory, and will be here called the 'transition wavelength.' Its significance and magnitude will be discussed in section 17.

The solution of (34) and (35) is

$$a_R = \frac{l^2}{l^2 + l_0^2}\, a(h, k) \tag{37}$$

$$a_P = \frac{l_0^2}{l^2 + l_0^2}\, a(h, k) \tag{38}$$

These equations give the separate contributions of regelation and plastic flow to the accommodation of the glacier to its bed at any wavelength.

The pressure distribution $P_0(x, y)$ for combined regelation and plastic-flow sliding can now be calculated from (31) by obtaining $\Pi(h, k)$ either from (32) and (37) or from (33) and (38):

$$\Pi(h, k) = 2\eta v i \frac{h l l_0^2}{l^2 + l_0^2}\, a(h, k) \tag{39}$$

8. BASAL SHEAR STRESS

The pressure distribution $P_0(x, y)$ given by (30) and (39) results in a drag exerted by the ice on bedrock. The average drag force per unit area of the x, y plane is the basal shear stress τ, which must equal the driving stress for sliding at the observed velocity. (The driving stress is in practice the result of body forces applied to the entire ice mass.) The average drag force per unit area is the average of the x component of $P_0(x, y)$ applied to the surface $z_0(x, y)$. If $\mathbf{dS}$ is

an element of area of this surface, expressed as a vector along the upward-directed normal, and if $\mathbf{e}_x$ is a unit vector in the x direction, then

$$\tau = -\frac{1}{A}\int_{z_0} P_0\mathbf{e}_x\cdot d\mathbf{S} = \frac{1}{A}\iint_A P_0(x, y)\frac{\partial z_0}{\partial x}\,dx\,dy$$

$$= \langle P_0\,\partial z_0/\partial x\rangle \tag{40}$$

For bedrock topography of general form, (40) in combination with (30), (39), and (3) gives

$$\tau = \frac{1}{A}\int_{-\infty}^{+\infty}\int dx\,dy\,\frac{A}{4\pi^2}\iint_{-\infty}^{+\infty} 2\eta v i h l\,\frac{l_0^2}{l^2+l_0^2}\,a(h, k)e^{i(hx+ky)}\,dh\,dk$$

$$\cdot\frac{A}{4\pi^2}\iint_{-\infty}^{+\infty} ih'a(h', k')e^{i(h'x+k'y)}\,dh'\,dk' \tag{41}$$

By standard Fourier manipulations, (41) reduces to

$$\tau = \frac{A}{4\pi^2}\iint_{-\infty}^{+\infty} 2\eta v h^2 l\,\frac{l_0^2}{l^2+l_0^2}\,a^2(h, k)\,dh\,dk \tag{42}$$

Introducing into (42) the roughness spectral function $\zeta(h, k)$ defined in (6), we get

$$\tau = \frac{8\pi}{3}v\iint_{-\infty}^{+\infty}\frac{h^2l_0^2}{l^3(l^2+l_0^2)}\,\eta\zeta^2(h, k)\,dh\,dk \tag{43}$$

When the bedrock topography is isotropic, so that $\zeta(h, k)$ depends on l only, (43) becomes

$$\tau = \frac{8\pi^2}{3}v\int_0^\infty \frac{l_0^2}{l^2+l_0^2}\,\eta\zeta^2(l)\,dl \tag{44}$$

The integral in (44) does not diverge when $\zeta(l)$ is constant, independent of l, that is, for a white roughness spectrum as defined in section 4. From (43) or (44) it follows that τ is insensitive to $\zeta(h, k)$ or $\zeta(l)$ for $l \ll l_0$ and for $l \gg l_0$; truncation of the roughness spectrum below a wavelength $\lambda_1 \ll \lambda_0$ or above a wavelength $\lambda_2 \gg \lambda_0$, as discussed in section 4, has no effect on τ. The integral in (44) converges at the upper limit if the asymptotic form of $\zeta(l)$, as $l \to \infty$, is $|\zeta(l)| \sim l^s$ with $s < \frac{1}{2}$, and it converges at the lower limit if, as $l \to 0$, $|\zeta(l)| \sim l^s$ with $s > -\frac{1}{2}$. The condition $|\zeta(l)| =$ constant ($s = 0$) thus lies at the middle of the parameter range $-\frac{1}{2} < s < \frac{1}{2}$ for convergence of (44). In this sense the white roughness spectrum, introduced in section 4 on an entirely different basis, is a natural one for the basal sliding phenomenon.

For the white spectrum, we obtain from (44) the simple result

$$\tau = (4\pi^3/3)\eta l_0\zeta^2 v \tag{45}$$

9. STRAIN-RATE DISTRIBUTION

To provide a basis for considering the nonlinear flow problem in section 10, we discuss here the strain-rate distribution implied by the linear theory in sections 6 and 7. The strain-rate components $\dot{e}_{ij}$ derived from equation 24 (after Fourier synthesis) can be summarized as follows:

$$\dot{e}_{ij} = \frac{A}{4\pi^2}\iint_{-\infty}^{+\infty} b_{ij}C(h, k)ze^{-lz}e^{i(hx+ky)}\,dh\,dk \tag{46}$$

where $b_{ij} = -t_it_j$ and $t_1 = -ih$, $t_2 = -ik$, $t_3 = l$. The coefficients $C(h, k)$ in (46) are given, from (29) and (38), by

$$C(h, k) = iv\,\frac{hl_0^2}{l^2+l_0^2}\,a(h, k) \tag{47}$$

A useful measure of the over-all rate of deformation at any point is the second strain-rate tensor invariant:

$$\dot{\epsilon} = (\tfrac{1}{2}\dot{e}_{ij}\dot{e}_{ij})^{1/2} \tag{48}$$

(Summation over repeated subscripts is understood.) For a single Fourier component, the $\dot{e}_{ij}$ values from (46) give, when substituted in (48),

$$\dot{\epsilon} = |C|l^2ze^{-lz} \tag{49}$$

so that, for a single Fourier component, $\dot{\epsilon}$ shows no dependence on x or y. For the general field of flow described by (46), a pertinent measure of the deformation rate at distance z from the ice-bedrock interface is the mean square value of $\dot{\epsilon}$, averaged over x and y. From (46), this is

$$\langle\dot{\epsilon}^2\rangle = \frac{1}{A}\iint\frac{1}{2}\dot{e}_{ij}\dot{e}_{ij}\,dx\,dy = \frac{1}{2}\frac{A}{4\pi^2}\iint_{-\infty}^{+\infty} b_{ij}b_{ij}{}^*z^2e^{-2lz}CC^*\,dh\,dk$$

$$= \frac{A}{2\pi^2}z^2\iint l^4e^{-2lz}CC^*\,dh\,dk \tag{50}$$

Introducing (47) and (6),

$$\langle\dot{\epsilon}^2(z)\rangle = \frac{8\pi}{3}v^2z^2\iint_{-\infty}^{+\infty}\frac{h^2l_0^4}{(l^2+l_0^2)^2}\,e^{-2lz}\zeta^2(h, k)\,dh\,dk \tag{51}$$

For a white roughness spectrum, (51) reduces to

$$\langle\dot{\epsilon}^2(z)\rangle^{1/2} = \tfrac{2}{3}{}^{1/2}\pi v\zeta l_0\Xi(2l_0z) \tag{52}$$

where

$$\Xi^2(p) = p^2\int_0^\infty e^{-p\eta}\,\eta^3\,d\eta/(1+\eta^2)^2 \tag{53}$$

The integral in (53) can be evaluated to give

$$\Xi^2(p) = \tfrac{1}{2}p^2\frac{d^2}{dp^2}(\sin p\,\mathrm{ci}\,p + \cos p\,\mathrm{si}\,p) \tag{54}$$

where si p and ci p are the following functions, defined by *Jahnke and Emde* [1945, p. 3]:

$$\text{si } p = -\int_p^\infty \frac{\sin \xi}{\xi}\, d\xi$$

$$\text{ci } p = \int_p^\infty \frac{\cos \xi}{\xi}\, d\xi$$

The z dependence of $\langle \dot{\epsilon}^2 \rangle^{1/2}$ is contained in the function $\Xi(2l_0 z)$, which is plotted in Figure 2. The rms strain-rate invariant $\dot{\epsilon}$ rises from 0 at the ice boundary to a maximum ($\Xi_{max} = 0.419$) at $l_0 z = 0.883$, and then decreases asymptotically toward 0 at large z. For comparison, Figure 2 also shows the function $\dot{\epsilon}(z)$ obtained from (49) for $l = l_0$, and normalized to the same maximum value as Ξ in (53). The two strain-rate distributions are similar, conforming to the fact that the greatest strain-rate contributions are from wavelengths near λ_0. The maximum of the composite distribution is flatter and is shifted slightly toward the ice-bedrock interface. At large z the composite distribution approaches zero more slowly than the distribution for the single wave number $l = l_0$. For large p, $\Xi(p) \to 6^{1/2}/p$.

To the strain-rate distribution in (51) must be added, for completeness, a contribution due to the shear flow under the basal shear stress τ. It has been shown (W. D. Harrison, unpublished data, 1969) that, for a single roughness wavelength (and for $k = 0$), the added term, to lowest order in the roughness, has the form

$$+\tfrac{1}{4} h^6 a_P{}^4 v^2 [1 + (1 - 2hz)^2 e^{-4hz}] \tag{55}$$

the basal shear stress being given by

$$\tau = \eta h^3 a_P{}^2 v \tag{56}$$

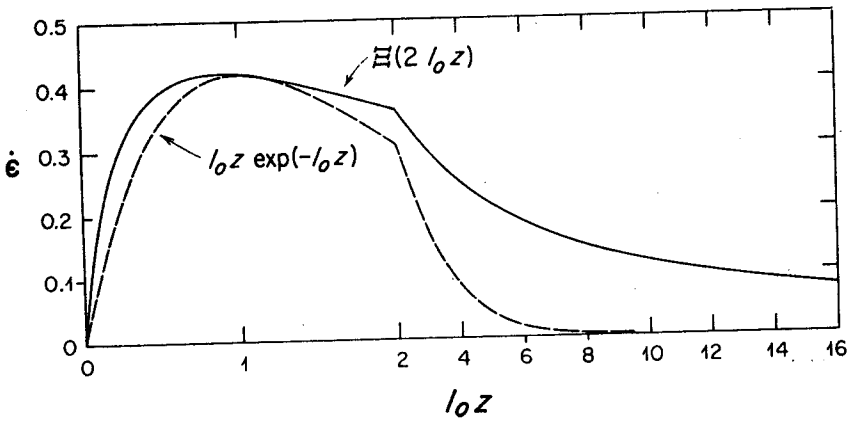

Fig. 2. Comparison of the strain-rate distributions for white roughness and for a single roughness wavelength at $\lambda = \lambda_0$. For white roughness, the rms strain rate $\langle \dot{\epsilon}^2(z) \rangle^{1/2}$ from (52) is plotted in terms of the dimensionless function $\Xi(2l_0 z)$. For the single wavelength, the strain-rate distribution from (49) is shown as scaled so that the two strain-rate distributions have the same peak value. The abscissa changes scale at $l_0 z = 2$.

Relative to the flow contributions in (51), the term (55) is of second order in the roughness, so that for low roughness it is a small correction. If for simplicity, therefore, the z- and h-dependent factor in brackets in (55) is ignored (it contributes only near $z = 0$), the shear-flow contribution to $\langle \dot{\epsilon}^2 \rangle$ is simply $(\tau/2\eta)^2$. Since this contribution is independent of the details of the roughness spectrum, it can be included in the complete flow field simply by modifying (51) as follows:

$$\langle \dot{\epsilon}^2 \rangle = \frac{8\pi}{3} v^2 z^2 \int\int_{-\infty}^{+\infty} \frac{h^2 l_0{}^4}{(l^2 + l_0{}^2)^2} e^{-2lz} \zeta^2(h, k)\, dh\, dk + \left(\frac{\tau}{2\eta}\right)^2 \tag{57}$$

10. RHEOLOGICAL NONLINEARITY

The linear relation (43) between sliding velocity v and shear stress τ reflects the linear flow behavior assumed in (23). For ice, which behaves as a nonlinear, generalized Newtonian fluid, the appropriate relation between stress and strain rate is the same as (23), except that η is no longer a constant, but is instead a function of the strain-rate invariant $\dot{\epsilon}$ defined in (48). The commonly observed 'power-law' dependence of η on $\dot{\epsilon}$ can be expressed

$$\eta = N \dot{\epsilon}^{-\alpha} \tag{58}$$

where α and N are constants, α being related to the exponent n in the nonlinear relation strain rate $\sim$ (stress)^n by

$$\alpha = 1 - 1/n \tag{59}$$

An exact solution to the nonlinear flow problem, corresponding to (22) for linear rheology, does not exist. We here develop an approximate treatment that uses the linear theory in sections 6–9 as a starting point, and that is able to take into account the nonlinearity to the fullest extent possible while retaining the basic advantages of the Fourier-analytic approach used in sections 4–9.

The motivation for the approximate solution comes from (49), which suggests that, since $\dot{\epsilon}$ is independent of x and y for a single Fourier component in the linear theory, it may also be approximately so for nonlinear flow. If this were true, then η as given by (58) would depend only on z. Now it can be shown that if a half-space in which η varies only with z is subjected to a sinusoidal distribution of normal stress τ_{zz} at the boundary $z = 0$, the response will be a sinusoidal distribution of normal velocity u_z. For Fourier components individually, there will exist a relationship of the form (26), except that the η in (26) will be replaced by a function of l that depends on the viscosity distribution $\eta(z)$. The existence of this relationship allows the Fourier-analytic technique to be applied in a straightforward way to the sliding problem, because the separate Fourier components do not then couple to one another via the boundary conditions at $z = 0$, and the relationship between regelation and plastic flow is determined separately for the individual Fourier components, as is shown in section 7. This state of affairs does not imply that the flow solutions for the different Fourier components can be superposed, because these are coupled to one another via their contributions to $\dot{\epsilon}(z)$ and hence to $\eta(z)$ from (58).

A detailed development of the points in the foregoing paragraph is rather lengthy, and is given in a separate paper [*Kamb*, 1970]. We develop here the simplest possible treatment consistent with the basic assumption that the nonlinear flow is dominated by an effective viscosity distribution $\eta(z)$ that is a function of z only. To do this we must propose both a method for calculating $\eta(z)$, and an appropriately modified form of (26) that takes into account this $\eta(z)$.

It is intuitively reasonable to suppose that for a given Fourier component, a relation like (26) between normal velocity and normal stress at the boundary is determined primarily by the effective viscosity $\eta(z)$ in that region of the half-space where the deformation rates for this Fourier component are the greatest, namely near $z = l^{-1}$, where, for the linear theory as given by (49), $\dot{\epsilon}$ is a maximum. Specifically we will assume that for each individual Fourier component

$$\tau_{zz}(x, y, 0) = -2\eta(l^{-1})lu_z(x, y, 0)$$

or, expressed in terms of the Fourier coefficients used in (27) and (31):

$$\Pi_P(h, k) = 2\eta(l^{-1})lC(h, k) \tag{60}$$

In the more detailed treatment mentioned above [*Kamb*, 1970], it is shown that this assumption is valid to a satisfactory approximation. Equation 60 can be made exact by multiplying $\eta(l^{-1})$ by a correction factor R, whose value is derived in the detailed treatment. The value of R depends in general on the form of the roughness spectrum $\zeta(h, k)$ (which influences the form of the function $\eta(z)$) and on n in (58), but it does not depend only on the sliding velocity v or on the constant N in (58). For a roughness spectrum consisting of a single wavelength λ, R is independent of λ, and it is insensitive to n and ζ over the practically pertinent range of these parameters; its value is approximately 1.2, decreasing to about 1.1 for high $\zeta(\gtrsim 0.05)$. For a white roughness spectrum, R depends also on λ/λ_0, but the range of variation is not large: $R(0.1\lambda_0) \cong 1.4$, $R(\lambda_0) \cong 1.2$, $R(10\lambda_0) \cong 1.3$. In the simple treatment here we will omit the correction factor R, since its value is near 1, and since for the white roughness spectrum the resulting relation between v and τ proves to be insensitive to the value of R (Kamb, paper in preparation, 1970).

On the basis of (60), which replaces (26), the treatment in section 7 for linear flow becomes applicable to nonlinear flow, the constant η of (33), (36), and (39)–(44) being replaced by $\eta(l^{-1})$.

To calculate $\eta(z)$ accurately, we need to solve for the complete flow field due to a given velocity distribution on the boundary $z = 0$. This can be done for the individual Fourier components separately if the $\eta(z)$ is given in advance, but of course $\eta(z)$ must be determined by (58) from the strain-rate field that results from the complete calculation. In the detailed treatment (Kamb, paper in preparation, 1970), it is shown how this calculation can be performed by a somewhat lengthy iterative procedure. In the present approximate treatment, we avoid this calculation by making the simple assumption that, for the purpose of calculating the strain-rate distribution that determines $\eta(z)$, we can take the velocity distributions for the individual Fourier components to be the same as those given by the linear theory in (24). The results of the detailed treatment show that the actual strain-rate distribution is not modified in an important way from that obtained by this simple assumption; this is reflected in the fact that the correction factors R to be applied to (60) turn out to be near 1 when $\eta(l^{-1})$ is calculated on the basis of this assumption.

If $\dot{\epsilon}$ as calculated from the complete flow field were indeed independent of x and y, as it is in (49), the basic assumption of the approximate approach developed here would be exactly satisfied, and the solution given by the detailed treatment [*Kamb*, 1970] would be exact. The detailed treatment shows, however, that in general there must actually be some x and y dependence of $\dot{\epsilon}$; in fact, this can occur already in the linear theory, for certain combinations of Fourier components. To the basic assumption of the approximate treatment, that the flow is dominated by the z dependence of η, we must therefore add an assumption as to how any actual x and y dependence of $\dot{\epsilon}$ is effectively averaged over x and y, in the process that determines the appropriate $\eta(z)$. Since any such averaging process is determined in the last analysis by the complete 3-dimensional flow solution, we cannot give a rigorous justification for any particular averaging scheme within the framework of the present approximation. We will therefore make the assumption that leads to the simplest possible mathematical development when applied to a Fourier-analyzed velocity field: namely, that the $\dot{\epsilon}$ to be used in (58) is $\langle\dot{\epsilon}^2\rangle^{1/2}$, as defined first in (50) and as corrected for the presence of an over-all shear stress τ in the way shown in (57), where now, of course, the η that appears on the right side of (57) is $\eta(z)$.

The two assumptions made in the foregoing two paragraphs provide the basis for combining (57) and (58) to get an equation that determines $\eta(z)$ for the nonlinear flow:

$$\left(\frac{N}{\eta(z)}\right)^{2n/(n-1)} = \frac{8\pi}{3} v^2 z^2 \iint_{-\infty}^{+\infty} \frac{h^2 \mathcal{L}^4(l)}{(l^2 + \mathcal{L}^2(l))^2} e^{-2lz} \zeta^2(h, k)\, dh\, dk + \left(\frac{\tau}{2\eta(z)}\right)^2 \tag{61}$$

The quantity l_0 that occurs in (57) has been replaced in (61) by the function $\mathcal{L}(l)$. Whereas in the linear theory l_0 is a constant, defined in (36), in the nonlinear case it becomes dependent on wave number l. This dependence arises through the appearance of $\eta(l^{-1})$ in (36), which we rewrite as

$$\mathcal{L}^2(l)\eta(l^{-1}) = \Gamma \equiv \frac{H}{2C_0(K_1 + K_2)} \tag{62}$$

To make evident the distinction between the constant l_0 of the linear theory and the wavelength-dependent quantity given by (62) in the nonlinear theory, we replace the symbol l_0 by $\mathcal{L}(l)$. By the same token, l_0 in (37)–(44) must be replaced by $\mathcal{L}(l)$ in the nonlinear theory, and η must be replaced by $\eta(l^{-1})$. With (62), (43) thus becomes

$$\tau = \frac{8\pi}{3} v\Gamma \iint_{-\infty}^{+\infty} \frac{h^2 \zeta^2(h, k)}{l^3(l^2 + \mathcal{L}^2(l))}\, dh\, dk \tag{63}$$

Equations (61), (62), and (63) can now be combined to give

$$\left(\frac{N}{\eta(z)}\right)^{2n/(n-1)} = \frac{8\pi}{3} v^2 z^2 \iint_{-\infty}^{+\infty} \frac{h^2 \zeta^2(h, k)}{(l^2 \eta(l^{-1})/\Gamma + 1)^2} e^{-2lz}\, dh\, dk + \left[\frac{4\pi}{3} \frac{v}{\eta(z)} \iint_{-\infty}^{+\infty} \frac{\Gamma h^2 \zeta^2(h, k)}{l^3(\Gamma/\eta(l^{-1}) + l^2)}\, dh\, dk\right]^2 \quad (64)$$

The general form of the solutions to be derived from (64) can be found by nondimensionalizing in the following way. Let us introduce a wave-number parameter l_α defined as

$$l_\alpha \equiv (\Gamma/N)^{n/(n+1)} (\zeta_0 v)^{(n-1)/(n+1)} \quad (65)$$

Nondimensional wave-number components are then defined as

$$\mu = l/l_\alpha \qquad \mu_x = h/l_\alpha \qquad \mu_y = k/l_\alpha$$

and a nondimensional z coordinate as

$$\xi = l_\alpha z$$

The quantity ζ_0 in (65) is to be a normalizing constant for the roughness spectrum, so that the normalized spectrum $Z(\mu_x, \mu_y)$ is given by

$$Z(\mu_x, \mu_y) \equiv \zeta(h, k)/\zeta_0$$

ζ_0 represents the general magnitude of the roughness (for example, the maximum value of $\zeta(h, k)$), and $Z(\mu_x, \mu_y)$ describes the relative spectral distribution of roughness, without regard to magnitude. Now we define a nondimensionalized reciprocal viscosity function $\varphi(\xi)$ by

$$\varphi(\xi) \equiv \Gamma/l_\alpha^2 \eta(z) \quad (66)$$

When the above substitutions are made into (64), the following nondimensional equation for $\varphi(\xi)$ results:

$$(\varphi(\xi))^{2n/(n-1)} = \frac{8\pi}{3} \xi^2 \iint_{-\infty}^{+\infty} \frac{\mu_x^2 e^{-2\xi\mu} Z^2(\mu_x, \mu_y)}{(\mu^2/\varphi(\mu^{-1}) + 1)^2}\, d\mu_x\, d\mu_y + \frac{16\pi^2}{9} \zeta_0^2 (\varphi(\xi))^2 \left(\iint_{-\infty}^{+\infty} \frac{\mu_x^2 Z^2(\mu_x, \mu_y)}{\mu^3(\mu^2 + \varphi(\mu^{-1}))}\, d\mu_x\, d\mu_y\right)^2 \quad (67)$$

Equation (67) shows that the viscosity distribution $\varphi(\xi)$ depends on the spectral distribution of roughness $Z(\mu_x, \mu_y)$, and also to some extent on the magnitude of the roughness ζ_0, via the second term on the right. Once $\varphi(\xi)$ is determined from (67), the relationship between shear stress and sliding velocity can be obtained from (63):

$$\tau = \frac{4\pi}{3} \left(\frac{N}{\Gamma}\right)^{n/(n+1)} v^{2/(n+1)} \zeta_0^{(n+3)/(n+1)} \iint_{-\infty}^{+\infty} \frac{\mu_x^2 Z^2(\mu_x, \mu_y)\, d\mu_x\, d\mu_y}{\mu^3(\mu^2 + \varphi(\mu^{-1}))} \quad (68)$$

The form of the dependence of shear stress on sliding velocity given by (68) appears at first sight to be the same as that obtained originally by *Weertman* [1957], but in fact this dependence follows only if $|Z(\mu_x, \mu_y)|$ is a constant. Otherwise, the variation with v of the scaling parameter l_α in (65) causes a shift in the function $Z(\mu_x, \mu_y)$ as v changes, and thus introduces an additional v dependence into (68).

The integral equation (67) is probably sufficient in principal to define the viscosity function $\varphi(\xi)$ or $\eta(z)$ for arbitrary $\zeta(h, k)$. A direct solution of (67) does not appear to be feasible, even for simple functions $Z(\mu_x, \mu_y)$, but numerical solution could probably be achieved. However, in evaluating the theory here for particular types of roughness spectrum $\zeta(h, k)$, as is done in sections 11–13, we will make one additional symplifying approximation, which makes it possible to avoid the numerical solution of (67). This approach also has the advantage that it brings out the physical significance of the nondimensionalizing parameters l_α and Γ/l_α^2 introduced in (65) and (66).

The additional approximation is to simplify the calculation of $\langle \dot{\epsilon}^2(z) \rangle$ on the right-hand side of (61) by ignoring the variation of $\mathcal{L}$ with l under the integral signs. Under the integral signs we replace $\mathcal{L}(l)$ by the constant l_α, whose value is now to be determined not by (65), but by a suitable argument for each type of roughness spectrum separately. The replacement $\mathcal{L}(l) \to l_\alpha$ in (61) has the effect of simplifying the calculation of $\langle \dot{\epsilon}^2(z) \rangle$ to the same problem encountered in the linear theory, which leads to the result given in (51), where now, however, l_0 must be replaced by l_α. The quantity l_α must be chosen so that (51) gives the best possible approximation to the strain-rate distribution for nonlinear flow. Since in fact $\mathcal{L}(l)$ is governed by (62), l_α should be chosen to give a close approximation to $\mathcal{L}(l)$ over that part of the spectrum where the effect of $\mathcal{L}(l)$ on the integrals in (61) and (63) is most important.

Although in the nonlinear theory, as is shown by (62), there is no single transition wavelength λ_0, as there is in the linear theory from (36), nevertheless we can identify $\lambda_\alpha = 2\pi/l_\alpha$ as the effective transition wavelength in that part of the wavelength spectrum that is most important to the sliding process.

11. WHITE ROUGHNESS

For $|\zeta(h, k)| = \zeta =$ constant, all roughness wavelengths contribute on an equal basis to (51), and from the occurrence of the ratio $\mathcal{L}^2/(l^2 + \mathcal{L}^2)$ in this equation it is clear that the value of $\mathcal{L}(l)$ is most important for $l \approx \mathcal{L}$. We therefore define l_α self-consistently as the value of l such that $\mathcal{L}(l_\alpha) = l_\alpha$. From (62), this means that

$$l_\alpha^2 \eta(l_\alpha^{-1}) = \Gamma \quad (69)$$

For white roughness, (51) gives the results in (52)–(54), in which we must replace l_0 by l_α. The use of these results in place of the integral in (61) neglects the influence on $\langle \dot{\epsilon}^2(z) \rangle$ of the variation of $\mathcal{L}$ with l, but it assigns the correct value to $\mathcal{L}$ near $l = l_\alpha$, where the effect of $\mathcal{L}$ on $\langle \dot{\epsilon}^2(z) \rangle$ is the greatest.

Under the same approximation, the value of τ in (61) is to be calculated from (63) with $\mathcal{L}(l)$ replaced by l_α, and with $|\zeta(h, k)| = \zeta$:

$$\tau = (4\pi^2/3)\, \Gamma(v\zeta^2/l_\alpha) \quad (70)$$

Putting (52) and (70) into (61) in the way described, we obtain, in place of (64),

$$\left(\frac{N}{\eta(z)}\right)^{2n/(n-1)} = \frac{4}{9}\pi^6 v^2 \zeta^2 l_\alpha^2 \left[\Omega(2l_\alpha z) + \zeta^2\left(\frac{\eta(l_\alpha^{-1})}{\eta(z)}\right)^2\right] \tag{71}$$

where $\Omega(p) \equiv (3/2\pi^4)\Xi^2(p)$. To determine l_α, we put $z = l_\alpha^{-1}$ in (71) and then substitute $\eta(l_\alpha^{-1})$ from (69) into (71):

$$l_\alpha = (\Gamma/N)^{n/(n+1)}[\tfrac{2}{3}\pi^3(\Omega(2) + \zeta^2)^{1/2}\zeta v]^{(n-1)/(n+1)} \tag{72}$$

where $\Omega(2) = 2.68 \times 10^{-3}$. Equation (72) shows how the quantity l_α, which for linear rheology ($\alpha = 0$) is a material constant Γ/N, depends in the nonlinear case ($\alpha > 0$) on roughness ζ and sliding velocity v (α is related to n by equation 59). As is expected, the effective transition wavelength λ_α decreases with increasing ζ and v, which corresponds to increasing plastic flow rates in the ice.

By comparing (72) and (65), it is seen that l_α as defined here is the same, except for a numerical factor, as the l_α defined in section 10 for purposes of nondimensionalization. From (69), the quantity Γ/l_α^2 that appears in (66) is just $\eta(l_\alpha^{-1})$, except for a numerical factor.

Once l_α is known from (72) (and then $\eta(l_\alpha^{-1})$ from equation 69), $\eta(z)$ can in principle be calculated from (71), but a simple solution of (71) in closed form is not available for arbitrary values of n. To express (71) in the form best suited to calculation, let

$$\mathfrak{L}^2(l)/l_\alpha^2 = \eta(l_\alpha^{-1})/\eta(l^{-1}) \equiv X \tag{73}$$

Dividing (71) by the same equation evaluated at $z = l_\alpha^{-1}$, we obtain for X the following equation, which constitutes a simplified version of (67):

$$X^{2n/(n-1)} \quad \frac{\Omega(2l_\alpha/l) + \zeta^2 X^2}{\Omega(2) + \zeta^2} \tag{74}$$

From the form of (74) it is clear that X as defined in (73) depends only on the variables l/l_α and ζ, so we write $X = X(l/l_\alpha, \zeta)$. Curves showing X as a function of l/l_α, for several values of ζ over the range of practical importance, are given in Figure 3, as calculated from (74). (The curves as labeled in Figure 3 give $\eta(z)/\eta(l_\alpha^{-1})$ as a function of $l_\alpha z$; because of the correspondence $z \to l^{-1}$, the axes in Figure 3 can be relabeled so that the curves give X as a function of l/l_α.) For practical purposes X has the maximum value 1.0, which is attained over a range of l/l_α values near 1. For small l/l_α (long wavelengths), X approaches a constant value given by

$$X^{-1} \to \eta(\infty)/\eta(l_\alpha^{-1}) = (\Omega(2)/\zeta^2 + 1)^{(n-1)/2} \tag{75}$$

and the same limit is approached as $l \to \infty$.

The basal shear stress can now be calculated from (63):

$$\tau = \frac{8\pi^2}{3}\Gamma v \zeta^2 \int_0^\infty \frac{dl}{l^2 + \mathfrak{L}^2(l)} \tag{76}$$

The dependence of $\mathfrak{L}$ on l in the denominator of (76) is important for small l, where the viscosity ratio can show a large change from the value near l_α as indicated

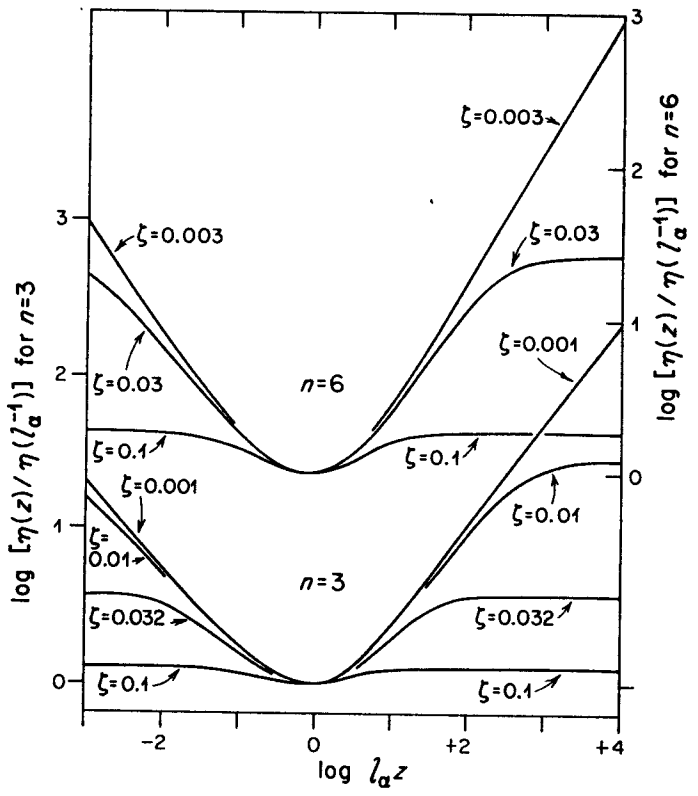

Fig. 3. Depth dependence of the effective viscosity $\eta(z)$, from (74). The viscosity distribution is plotted for $n = 6$ (above) and $n = 3$ (below), and for a range of roughness values ζ. The ordinate scales for $n = 3$ and $n = 6$ are displaced and are read on the left and right, respectively.

by (75). If we define the function

$$G(\zeta\,; n) = \frac{2}{\pi}\int_0^\infty \frac{d\mu}{\mu^2 + X(\mu, \zeta)} \tag{77}$$

then the shear stress given in (76) can be written

$$\tau = \frac{4\pi^3}{3}\Gamma\frac{\zeta^2 v}{l_\alpha} G(\zeta\,; n) \tag{78}$$

The function $G(\zeta; n)$ contains the effect on τ of the variation of $\mathfrak{L}$ with l or of η with z. It is given in Figure 4, as calculated from (74) and (77) for several values of n.

Combining (72) and (78), we obtain the final result for the relation between sliding velocity and basal shear stress:

$$\tau = 2\left(\frac{2\pi^3}{3}\right)^{2/(n+1)} \Gamma^{1/(n+1)} N^{n/(n+1)} \frac{G(\zeta; n)\zeta^{(n+3)/(n+1)}}{(\Omega(2) + \zeta^2)^{(n-1)/2(n-1)}} \cdot v^{2/(n+1)} \tag{79}$$

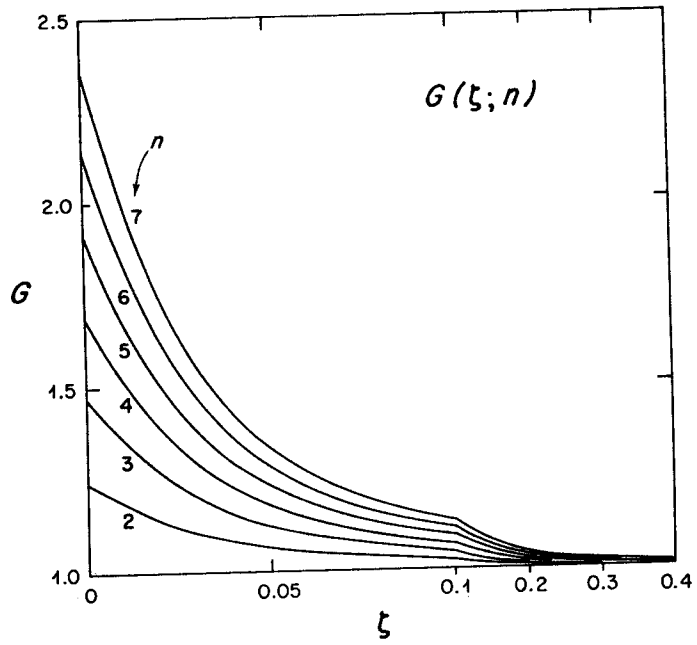

Fig. 4. The function $G(\zeta; n)$ that appears in (79), calculated from (74) and (77) for several values of n. The abscissa changes scale at $\zeta = 0.1$.

As was noted in section 10, the $\tau^{\frac{1}{2}(n+1)}$ dependence of v on τ in the white roughness case, given by (79), is the same as that found by *Weertman* [1957]. The source of the nonlinearity is basically the same in Weertman's treatment and in the present one. By comparing (79) and (78), it is seen that the nonlinearity enters via the dependence of the transition wavelength λ_α on the sliding velocity, as given by (72). The dependence of v on roughness is different in Weertman's treatment and the present one, because of the different nature of the roughness parameters for the two very different models of bedrock topography.

12. TRUNCATED WHITE ROUGHNESS SPECTRUM

In bedrock topography that has been subjected to extensive glacial abrasion, roughness is typically absent at wavelengths comparable to the transition wavelength and shorter (see sections 15–18). To represent this common state of affairs, we choose a white roughness spectrum that is truncated at a lower wavelength limit λ_L (wave number limit l_L). The abrupt truncation is doubtless a somewhat artificial feature, but it is chosen here as the simplest representation in the absence of any detailed quantitative knowledge of topographic roughness spectra.

If the truncation wavelength λ_L is greater than the effective transition wavelength $2\pi/\mathfrak{L}(l)$ for any l that occurs in the spectrum ($l < l_L$), then $\mathfrak{L}(l)$ has the

largest effect on (63) at $l = l_L$. Hence the appropriate definition of l_α in this case is

$$l_\alpha = \mathfrak{L}(l_L) \tag{80}$$

In calculating the strain-rate invariant $\langle \dot{\epsilon}^2(z) \rangle$, the integrals that appear via (61) in (53) and (63) are modified by replacing the upper limit ∞ by l_L, because of the truncation. From (61), simplified as explained in section 10, there then results the following relationship, serving to determine $\eta(z)$.

$$(N/\eta(z))^{2n/(n-1)} = \tfrac{2}{3}\pi^2 v^2 \zeta^2 l_\alpha{}^2 F(2l_\alpha z,\ l_L/l_\alpha) + (8\pi^2/3)\zeta^2(\tan^{-1} l_L/l_\alpha)^2(\eta(l_L{}^{-1})/\eta(z))^2 \tag{81}$$

where

$$F(p, q) = p^2 \int_0^q e^{-p\mu}\, \mu^3\, d\mu/(1 + \mu^2)^2 \tag{82}$$

Equation 81 can be considerably simplified if l_L is enough smaller than l_α to allow $\tan^{-1} l_L/l_\alpha$ to be replaced by l_L/l_α as an adequate approximation, and if in a similar approximation the quantity μ^2 in the denominator of the integral in (82) can be omitted. Representing the viscosity in terms of the ratio

$$\eta(l_L{}^{-1})/\eta(l^{-1}) \equiv V(l/l_L, \zeta) \tag{83}$$

the function V then satisfies

$$V^{2n/(n-1)} = \frac{\Theta(l/l_L) + \zeta^2 V^2}{\Theta(1) + \zeta^2} \tag{84}$$

and is hence a function only of l/l_L and ζ^2, as noted in (83). The function $\Theta(p)$ in (84) is

$$\Theta(p) = \frac{3}{16\pi^2} p^2 \left[3 - \left(3 + \frac{6}{p} + \frac{6}{p^2} + \frac{4}{p^3}\right) e^{-2/p}\right] \tag{85}$$

and $\Theta(1) = 8.14 \times 10^{-3}$. The quantity $\eta(l_L{}^{-1})$ in (83) is given by

$$\eta(l_L{}^{-1}) = N[\tfrac{4}{3}\pi^2 l_L v \zeta(\Theta(1) + \zeta^2)^{1/2}]^{-1+1/n} \tag{86}$$

In (83)–(86), which follow from the simplification of (81) described, the quantity l_α has disappeared. Evidently this simplification corresponds to omitting the contribution of regelation to the sliding process. The basal shear stress calculated with this simplification will be larger than for combined plastic flow and regelation, but the increase will be small when the bedrock topography has appreciable roughness only at wavelengths substantially longer than typical transition wavelengths. Following (63), the shear stress is

$$\tau = \frac{8\pi^2}{3} \zeta^2 v \int_0^{l_L} \frac{\mathfrak{L}^2 \eta}{l^2 + \mathfrak{L}^2}\, dl \tag{87}$$

Again, for l_L enough smaller than typical $\mathfrak{L}$ values, we can omit the quantity l^2 in the denominator, and obtain

$$\begin{aligned} \tau &= \frac{8\pi^2}{3} \zeta^2 v \int_0^{l_L} \eta(l^{-1})\, dl \\ &= \frac{8\pi^2}{3} \eta(l_L{}^{-1}) l_L \zeta^2 v M(\zeta; n) \end{aligned} \tag{88}$$

where

$$M(\zeta; n) \equiv \int_0^1 d\mu / V(\mu, \zeta) \tag{89}$$

With (86), (88) becomes

$$\tau = 2\left(\frac{4\pi^2}{3}\right)^{1/n} \frac{M(\zeta; n)\zeta^{1+1/n}}{(\Theta(1) + \zeta^2)^{(n-1)/2n}} N l_L^{1/n} v^{1/n} \tag{90}$$

The τ^n dependence of v on τ described in (90) is notably different from the $\tau^{\frac{1}{2}(n+1)}$ dependence in (79). The cause of this difference is obviously the effect of the regelation process, which is absent in (90). The function $M(\zeta; n)$ is plotted in Figure 5 for several values of n.

Theoretical results given by *Weertman* [1969, equations 2–4] for cube-shaped obstacles with a size range truncated at a fixed small obstacle size Λ'

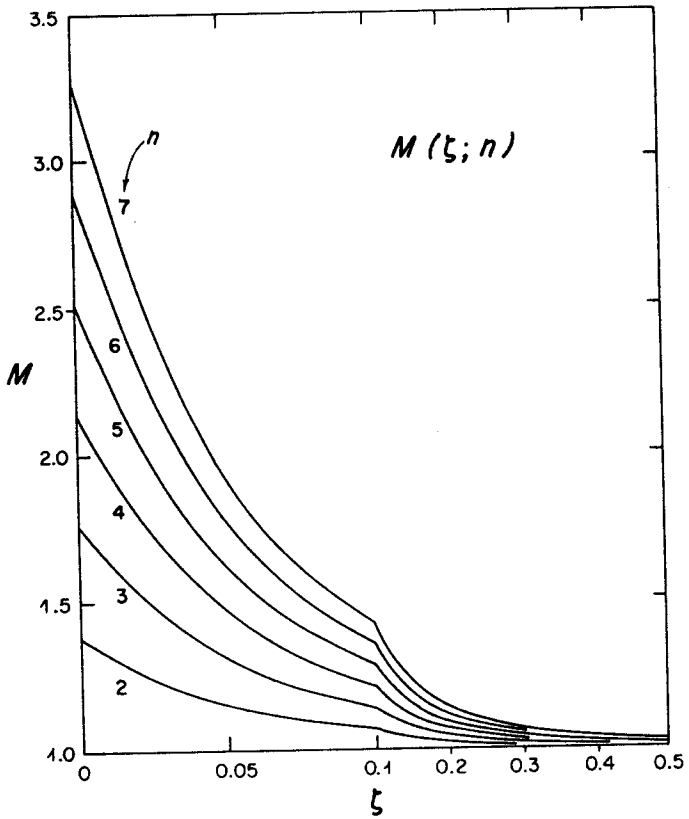

Fig. 5. The function $M(\zeta; n)$ in (90), calculated from (84) and (89) for several values of n. The abscissa changes scale at $\zeta = 0.1$.

(Weertman's notation) contain the implicit conclusion that v varies as τ^n, in agreement with (90) above. However, the agreement should really be expected only for Λ' significantly larger than the 'controlling' obstacle size Λ, rather than for Λ' as small as 0.1 Λ, the lower limit stated by *Weertman* [1964, p. 932]. The basis of this expectation is given in section 17, where the relation between Λ and λ_α is discussed.

13. SINGLE ROUGHNESS WAVELENGTH

An idealized form of bedrock topography consisting of a single sinusoid of wavelength λ and amplitude a serves as a useful comparison with the white roughness case, and can represent actual topography more accurately than a white roughness spectrum could in certain field examples where a well-defined roughness wavelength is locally recognizable. We take the wave crests to be normal to the sliding direction (hence $k = 0$). Since there is only one Fourier component, there is only one value of $\mathfrak{L}(l)$ in (61), and we therefore set

$$l_\alpha = \mathfrak{L}(h) = (\Gamma/\eta(h^{-1}))^{1/2} \tag{91}$$

The shear stress for a single wavelength can be extracted from (63) by using (2) and (6):

$$\tau = \frac{h^3 l_\alpha^{\,2}}{h^2 + l_\alpha^{\,2}} \eta(h^{-1}) a^2 v = 4\pi^2 \Gamma \frac{h}{h^2 + l_\alpha^{\,2}} \zeta^2 v \tag{92}$$

In obtaining (92), we introduce a single-wavelength roughness parameter

$$\zeta = a/\lambda \tag{93}$$

analogous to the parameter ζ introduced in (6) and (7) for a spectral distribution of roughness. For $h = l_\alpha$, (92) reduces to

$$\tau = 2\pi^2 \eta l_\alpha \zeta^2 v \tag{94}$$

Comparison of (94) and (45) shows that, in the linear theory ($\alpha = 0$), simple sinusoidal topography at the transition wavelength offers about half as much resistance to sliding as a white roughness topography of the same roughness, the roughness being as defined in (7) and (93).

Since for the single-wavelength spectrum the integral signs in (64) drop out, we can omit the type of simplification of (64) that is used in sections 11 and 12. Evaluating (64) at $z = h^{-1}$, we thus get

$$\langle \epsilon^2(h^{-1}) \rangle^{1/2} = \left(\frac{N}{\eta(h^{-1})}\right)^{n/(n-1)} = 2\pi \left(\frac{l_\alpha^{\,2}}{h^2 + l_\alpha^{\,2}} h\zeta v\right) (e^{-2} + \pi^2 \zeta^2)^{1/2} \tag{95}$$

l_α is determined by combining (91) and (95). The result is

$$\left(\frac{l_\alpha}{h}\right)^{2n/(n-1)} + \left(\frac{l_\alpha}{h}\right)^{2/(n-1)} = \left(\frac{\Gamma}{N}\right)^{n/(n-1)} \frac{2\pi}{e} (1 + \pi^2 e^2 \zeta^2)^{1/2} \zeta \frac{v}{h^{(n+1)/(n-1)}} \tag{96}$$

Once l_α is found from (96), τ can be calculated by substitution into (92). Since an explicit solution cannot in general be given for (96), the final shear stress formula cannot be obtained in closed form $\tau(v)$, but there are some limiting

cases that indicate aspects of the dependence of τ on v. The parameter l_α is a monotonically increasing function of v. For small enough v that $l_\alpha^2 \ll h^2$, the dependence of τ on v in (92) is linear. At these low shear stresses and sliding velocities, regelation dominates the sliding. At a v such that $l_\alpha = h$, we find from (92) and (96) that $d \ln v/d \ln \tau = \frac{1}{2}(n + 1)$, so that the apparent nonlinearity of the sliding velocity versus shear-stress curve is here the same as for the white roughness result in (79). At large v, where $l_\alpha^2 \gg h^2$, plastic flow dominates the sliding and τ is proportional to $v^{1/n}$, as in (90).

A slightly less idealized form of bedrock topography, but closely related to the single wavelength, consists of an array of humps formed by cross-corrugated sinusoidal waves of wavelength λ. Theoretical results for this topographic form, which is needed in the discussion of field observations, are given in equations (98)–(101) and (109).

14. EVALUATION WITH FIELD DATA

Applicability of the foregoing theory to the actual sliding phenomenon in nature is tested with the help of eight well-studied field examples (Table 1), covering a substantial range of conditions as to ice thickness, surface slope, shear strain rate in the basal ice, and sliding velocity. The sliding velocities for some of the examples were determined indirectly, from surveys of motion at the ice surface combined with internal deformation measured by borehole tilting (last column, Table 1). This indirect method can involve a substantial uncertainty owing to the required extrapolation from the deepest borehole measurement point to the actual bed (whose position is itself not generally known with the necessary accuracy). This source of uncertainty is serious only for example 8 in Table 1. The uncertainty is avoided by direct measurement of sliding velocity in tunnels, or by photography at the bottom of boreholes [*Harrison and Kamb*, 1970].

The shear stress τ at the base of the ice has not been measured directly; the available τ value used here is the average over the perimeter of the ice across each glacier cross section studied, which can be calculated from over-all mechanical equilibrium, ignoring any effect of longitudinal stresses. The f values in Table 1 are the ratios of hydraulic radius to depth for the channel cross sections, on the basis of which the average τ is calculated from the relation

$$\tau = f\rho_I g h_I \cos\theta \sin\theta \tag{97}$$

where θ is the slope of the glacier surface, and h_I is the ice depth measured vertically. The f value for examples 6 and 7 is valid for calculating τ at the borehole sites themselves, rather than as an average over the glacier cross section, because it is based on detailed knowledge of the distribution of flow velocity over the cross section [*Raymond*, 1969].

Uncertainty in f has little effect on evaluation of the sliding theory for any locality where the flow law was determined with the use of f, since both τ and N are then proportional to f; in (90), f then cancels out, and in (79), f enters only to the power $1/n$. The in situ ice flow-law parameters necessary in evaluating the sliding theory have been determined in the borehole experiments of examples 1 and 6–8. In the tunnel experiments (examples 3–5), the available strain-rate

TABLE 1. Summary of Field Examples

No.*	Locality	Surface Slope θ, deg	Depth h, meters	Basal Shear Strain Rate $\dot{\epsilon}_{xz}(0)$, yr^{-1}	f	Source of Flow Law	Source of v
1	Blue Glacier Hole K	13	116	0.60	0.75	Def. in holes K, P_2, N	Hole tilt + surf. vel.
2	Hole V	13	119	—	0.75	Def. in holes K, P_2, N	Borehole photography
3*a*	Western icefall	28	26	0.05	(1.0)	Assumed from K, P_2, N	Measmt. at tunnel head
3*b*	Western icefall	28	26	0.05	(1.6)†	Assumed from K, P_2, N	Measmt. at tunnel head
4	Central icefall, on bedrock ridge	40	64	0.8	0.61	Assumed from K, P_2, N	Measmt. at tunnel head
5	Central icefall, in bedrock trough	40	74	3.5	0.61	Assumed from K, P_2, N	Measmt. at tunnel head
6	Athabasca Glacier Hole 1B	3.9	316	0.045	0.5	Borehole def.	Hole tilt + surf. vel.
7	Hole 1A	3.9	311	0.054	0.5	Borehole def.	Hole tilt + surf. vel.
8	Hole 209	6.3	209	0.39	0.62	Borehole def.	Hole tilt + extrap. to bed

* 1. *Kamb and Shreve*, 1966.
2. *Harrison and Kamb*, 1970.
3. *Kamb and LaChapelle*, 1964.
4 and 5. *Kamb and LaChapelle*, 1968.
6 and 7. *Raymond*, 1969.
8. *Savage and Paterson*, 1963.

† Gives maximum τ consistent with $\dot{\epsilon}_{xz}(0)$ and flow law.

measurements do not allow as reliable a determination of the ice flow law, but they are found to be generally consistent with the flow law derived from the borehole experiments. Example 3*b* considers a τ value that is larger than that given by (97), and is the largest τ permissible, consistent with the detection limit for shear strain rate near the base of the ice in the tunnel.

The results of applying the sliding theory to the field examples in Table 1 are given in Tables 2–6. The quantities v, τ, N, and n in Table 2 are based on the field information noted above and in Table 1, and the remaining quantities are calculated from the theory. The necessary quantity Γ, defined in (62), depends on the conductivities of ice and bedrock. K_1 for ice is 0.005 cal sec^{-1} $°C^{-1}$ cm^{-1}. K_2 for bedrock at the actual field sites has not been measured; values for most

TABLE 2. Roughness ζ and Transition Wavelength λ_α Calculated from Theory for the Field Examples

Example	Field Data: v, m yr^{-1}	τ, bar	N, bar yr$^{1/n}$	n	White Spectrum: Full ζ	Full λ_α, cm	Truncated (λ_L = 3.54 m) ζ	Truncated λ_α, cm	Single Wavelength: $\lambda = \lambda_\alpha$ ζ	$\lambda = \lambda_\alpha$ λ_α, cm	λ = 5 m ζ	λ = 5 m λ_α, cm
1	22.3	1.7	0.884	5.25	0.019	13	0.049	32	0.048	7	0.098	20
					0.021	22	0.049	45	0.053	11	0.098	29
2	3.6	1.7	0.884	5.25	0.035	28	0.093	47	0.080	15	0.154	32
					0.040	45	0.093	67	0.088	25	0.154	45
3a	5.8	0.7	0.884	5.25	0.012	46	0.022	79	0.034	22	0.051	49
					0.014	76	0.022	112	0.037	37	0.051	69
3b	5.8	1.1	0.884	5.25	0.019	34	0.038	62	0.048	17	0.080	39
					0.021	56	0.038	88	0.053	28	0.080	55
4	128.	1.7	0.884	5.25	0.011	6	0.032	15	0.031	3	0.068	12
					0.013	10	0.032	28	0.034	5	0.068	17
5	3.6	2.0	0.884	5.25	0.041	24	0.134	37	0.091	13	0.194	27
					0.047	38	0.134	53	0.102	22	0.194	38
6	41.	0.95	1.32	3.0	0.007	31	0.018	50	0.015	21	0.029	38
					0.008	49	0.018	70	0.017	33	0.029	54
7	41.5	0.93	0.78	5.5	0.010	12	0.023	33	0.029	6	0.054	20
					0.011	21	0.023	47	0.031	10	0.054	28
8	3.	1.3	0.70	7.5	0.031	28	0.060	59	0.090	11	0.167	28
					0.035	15	0.060	84	0.099	18	0.167	40

The upper and lower values for each entry are for Γ = 155 and 77.5 bar yr m^{-2}, respectively.

of the pertinent rock types [*Clark*, 1966, p. 461 ff.] lie in the range 0.005–0.015 cal sec^{-1} °C^{-1} cm^{-1}, the larger values being shown particularly by water-saturated porous sandstones. The corresponding range of Γ values (for H = 73 cal cm^{-3}, C_0 = 0.0074 °C bar^{-1}) is Γ = 155 to 77.5 bar yr m^{-2}. In Tables 2, 4, and 6, the theoretically derived quantities are calculated for both of these limiting values of Γ, so as to include the range of results permissible within the uncertainty in Γ.

15. BEDROCK ROUGHNESS

The borehole experiments provide no direct evidence as to the roughness of the bed at the most pertinent wavelengths, of the order of a few meters or less. Attempts to obtain roughness information from borehole measurements have been made, but have not thus far been successful [*Fletcher and Kamb*, 1968; *Harrison and Kamb*, 1970]. The tunnel experiments give a sampling of the bedrock topography at the tunnel head, but the region sampled is generally much smaller than the area over which the bed roughness is effectively averaged in the sliding process (section 4). For these reasons, the most direct way to apply the sliding theory in the present state of knowledge is to calculate from the theory the bed roughness appropriate to each of the field examples. Results are given in Table 2 for four different assumptions as to the bedrock roughness spectrum $\zeta(h, k)$.

If we had no a priori information about details of the roughness spectrum, the most appropriate assumption would be a white spectrum, $|\zeta(h, k)|$ = constant = ζ, which does not single out any particular roughness wavelength as more important than any other. (A general indication of validity for roughness spectral functions of this type is provided by the power spectrum density data given by *Jaeger and Schuring* [1966] for four different topographic surfaces; none of them, however, are glacier beds.) The results of applying the theory for the white spectrum are derived from equations 72–79 with the stated values of the parameters. For comparison it is useful to consider an alternative extreme, in which only a single roughness wavelength is present. The most suitable wavelength for this purpose is λ_α, because, as is shown in section 17, the largest contribution to τ from the white roughness spectrum occurs at this wavelength. In Table 2 the results of evaluating ζ for a white roughness spectrum are compared with those for a single-wavelength spectrum with $\lambda = \lambda_\alpha$. The results for $\lambda = \lambda_\alpha$ are calculated from (92)–(96), with $h = l_\alpha$.

A more likely alternative to the white roughness spectrum can be formulated by considering the features shown by glaciated bedrock exposures; we can reasonably assume that bedrock surfaces under existing glaciers usually show similar features. The following statements are based on my own observations of glaciated bedrock outcrops, made over the period 1964–1970, with the express purpose of assessing the wavelength dependence of roughness. Bedrock surfaces that have been subjected to extensive glacial abrasion characteristically show prominent roughness wavelengths that are of the order of several meters along the direction of flow. In the direction of flow, there is typically an almost complete absence of roughness at wavelengths of half a meter or less. Transverse to the direction of flow, the roughness extends to shorter wavelengths, as repre-

sented by the typical longitudinal grooving and striations. However, the transverse roughness components have much less influence on the sliding process than do the longitudinal components. This is shown by the form of (43), in which, for fixed l, the contribution to τ from $\zeta^2(h, k)$ goes to zero as h goes to zero. Though the topographic anisotropy of the bedrock surface is thus significant here, the most important topographic feature is the absence of roughness at the shorter wavelengths along the direction of flow. In the absence of detailed information about the spectral function $\zeta(h, k)$, the most appropriate assumption is a truncated white spectrum that extends from long wavelengths down to a limiting wavelength λ_L that is of the order of several meters. Table 2 gives the results of applying the theory with $\lambda_L = 5/2^{1/2}$ meters, a cutoff wavelength that is chosen so that at $\lambda = 5$ meters the roughness appropriate to the parameter ζ is already fully developed, as is shown by the defining relation for ζ in (7). From the λ_α values in Table 2, it follows that λ_L is substantially greater than λ_α, hence the simplified theory in equations (83)–(90) is used in calculating the results for the truncated white spectrum in Table 2. Finally, the results for a single roughness wavelength with $\lambda = 5$ meters, calculated from (92)–(96) with $h = 2\pi/5$ m^{-1}, are given for comparison.

We now consider the significance of the ζ values in Table 2. With only a few exceptions, the ζ values are small (<0.1), so that the theoretical approach, based on small ζ (low roughness), is probably valid as a reasonable approximation. The range of derived ζ values is such that the first term almost always dominates the second on the right side of (61), so that the viscosity values are predominately determined by the stresses required for flow around the bedrock obstacles, rather than by the over-all basal shear stress τ. (The conditions for this are as follows: for white roughness, $\zeta < 0.052$; for truncated white roughness, $\zeta < 0.090$; for a single wavelength, $\zeta < 0.117$.)

A straightforward judgment as to whether the theory is quantitatively satisfactory could be made if we had test cases in which the actual bedrock roughness were known. Tunnel examples 3 and 5 come the closest to filling this need. A quantitative measurement of the roughness was not made, but, from the photographic record of the bedrock surface exposed at the tunnel heads [*Kamb and LaChapelle*, 1964, 1968], we can state the following facts: (1) effects of glacial abrasion are modest in these examples, and roughness is present at wavelengths down into the centimeter range and, locally, below; (2) in example 3, some bedrock roughness features in the form of cavities depressed below the general level of the bedrock surface are bridged over by the moving ice and therefore do not contribute to the roughness that is effective in offering resistance to sliding; (3) in example 5, the ice is in almost complete contact with the bed, only a few small cavities being bridged; (4) peak-to-trough amplitudes for individually recognizable roughness wave forms ($2a$ in equation 93) of about 0.1λ are abundant, and we can therefore expect that $\zeta(l)$ values of about 0.05 are appropriate for a representation of the bed; (5) the presence of structural features in the basal ice produced wholly by regelation in example 2 shows that, at least in this example, the range of significant roughness wavelengths extends down well below λ_α. For the conditions described, a white roughness spectrum is appropriate as a first approximation to the actual state of affairs. The white roughness ζ values calculated for example 5 (Table 2) are of the general magnitude expected ($\sim$0.05), whereas those for example 3 are definitely smaller (0.01–0.02), although not unreasonably so, in view of the greater extent of ice separation from bedrock. The single wavelength $\lambda = \lambda_\alpha$ roughness for example 3 is of the size expected, whereas that for example 5 is rather larger. When we consider the relatively small areas of the bed that could be sampled at the tunnel heads, and the consequent uncertainty as to whether the observed sample is fully representative of the bed over the larger area over which the roughness is effectively averaged in the sliding process (section 4), we can conclude that the bed roughness predicted by the theory for either the white roughness or the $\lambda = \lambda_\alpha$ models is generally reasonable in relation to the observed roughness.

A somewhat closer examination for example 3 is justified by the following observations [*Kamb and LaChapelle*, 1964]: (1) roughness waveforms of wavelength up to about 10 cm showed features of regelation sliding, without any effects of concommitant plastic-flow sliding; (2) roughness waveforms of wavelength $\sim$10 meters showed the effects of plastic-flow sliding; (3) there were no significant roughness waveforms of intermediate wavelength, in which combined effects of regelation and plastic-flow sliding could be observed. In view of these facts, it is more appropriate in comparing theory and observation for example 3 to calculate separately the effects due to waveforms of $\lambda \sim 10$ cm and of $\lambda \sim 10$ meters. Since the observed waveforms are in no case simple sine waves, it is somewhat more realistic for this purpose to represent the topography as an array of humps

$$z_0 = a \sin hx \sin hy \tag{98}$$

The results corresponding to (92), but for topography of the form (98), are as follows: for $h \gg l_\alpha$ (regelation sliding),

$$\tau = (\pi/2^{1/2})\,\Gamma a^2 v/\lambda \tag{99}$$

and for $h \ll l_\alpha$ (plastic-flow sliding)

$$\tau = 4 \cdot 2^{1/2}\pi^3 \eta a^2 v/\lambda^3 \tag{100}$$

in which η is given by (58) and $\dot{\epsilon}$ is obtained from

$$\langle \dot{\epsilon}^2(l^{-1})\rangle^{1/2} = \frac{4\pi^2}{e}\frac{a}{\lambda^2} v(1 + \tfrac{1}{2}e^2\pi^2\zeta^2)^{1/2} \tag{101}$$

(Equation 99 was given by *Kamb and LaChapelle* [1964].) For $\lambda = 2\pi/h = 10$ cm and $2a = 1$ cm, corresponding to the effects visible in Figure 3 (mislabeled Figure 6) of *Kamb and LaChapelle* [1964], equation 99 gives a contribution of 0.50 bar (for $K_2 = 0.005$ cal sec^{-1} °C^{-1} cm^{-1}) or 0.25 bar (for $K_2 = 0.015$) to the shear stress resisting sliding. For $\lambda = 10$ meters and $2a = 1$ meter, and with the flow-law parameters assumed in Table 2, equation 100 gives $\tau = 0.42$ bar. The combined resistance $\tau = 0.92$ or 0.67 bar is reasonable in relation to the range 0.7 to 1.1 bars estimated from the field information. It therefore appears

that the somewhat low values of ζ obtained in Table 2 by the evaluation of example 3 for a white roughness spectrum are a consequence of the fact that the actual roughness spectrum is more restricted as to available frequencies.

Example 4 in Table 2 is also based on observations at the head of a tunnel [*Kamb and LaChapelle*, 1968]. In this instance the ice was largely separated from the bed, and was resting on bedrock only at isolated points. Under these conditions it is not the bedrock roughness that is directly pertinent, but instead the roughness of the ice sole. Where unsupported, the sole showed no longitudinal roughness, whereas around the isolated points of support the local roughness was sometimes so large as to invalidate the theoretical approach used here. It is not possible to estimate quantitatively an effective average bed roughness under these circumstances, or to characterize reliably the spectral distribution of roughness. The over-all impression from the observations is of low sole roughness, and of a wide distribution of roughness wavelengths, with short-wavelength contributions necessary to account for the localized roughness around the isolated points of support. Of the spectrum models considered in Table 2, only the white roughness model could provide these features, but even this model is of dubious applicability under the extreme conditions prevailing. The white-roughness ζ values for example 4 in Table 2 are probably low enough to be reasonable as an over-all impression of the low average sole roughness.

For the examples in Table 2 based on borehole data, for which there is no direct information about the bed roughness, only general consideration as to the reasonableness of the results is possible. We first note some over-all features of the derived ζ values in Table 2. The ζ values for each spectrum model individually are relatively insensitive to the range of conditions in the different field examples, a wide range of sliding velocities and shear stresses being allowed by a relatively modest range of roughnesses. A similarly weak sensitivity of the calculated ζ to the parameters Γ, N, and n is also evident in Table 2. This behavior is a reflection of the nonlinearity in the basic equations 79, 90, and 92 + 96, under the large n values found in the borehole experiments. There is as much contrast among ζ values evaluated for a single field example with different spectrum models as among ζ values for the different field examples with a single model. For each field example, the ζ value derived for a single roughness wavelength at $\lambda = \lambda_\alpha$ is 2 to 3 times that for the white roughness spectrum. This is a consequence of the definitions of ζ for the two cases (equations 7 and 93) and the fact that, according to equation 108 below, significant contributions to the resisting stress τ are distributed over a wavelength range of several octaves above and below the octave containing λ_α. The truncated white roughness model, with $2^{1/2}\lambda_L = 5$ meters, requires ζ values comparable to those for the single wavelength at $\lambda = \lambda_\alpha$, and the single wavelength at $\lambda = 5$ meters requires ζ values about twice as large.

The appropriateness of the ζ values derived for the borehole examples in Table 2 can at present be judged only in relation to samples of bedrock topography visible around the periphery of the glaciers studied. On this basis, one expects that the truncated white roughness model should be appropriate. Roughness amplitudes $2a$ at wavelengths of about 5 meters are commonly ½ meter, hence we expect ζ to be about 0.05. This expectation is generally fulfilled by calculated ζ values for the borehole examples when interpreted with the truncated white spectrum, or with a single roughness wavelength at $\lambda = 5$ meters.

In the examples with relatively high sliding velocity (>20 m yr^{-1}), the theoretical ζ values required for a white roughness spectrum appear too small. This is particularly striking for examples 6 and 7. Local instances of bedrock topography with such a low roughness over a wide spectrum that includes 5- to 20-meter wavelengths certainly do occur, but, in my experience, they are rare. A possible explanation is that there is very extensive separation of the ice sole from the bedrock, perhaps like what was observed in field example 4. Although it is shown in section 19 that ice-bedrock separation can be an important feature of the sliding process under some circumstances, there is no direct evidence for the widespread presence of such extensive separation as is required to lower the effective roughness in examples 6 and 7 from the expected $\zeta \sim 0.05$ to the theoretically required $\zeta \sim 0.01$ over the whole spectral range. If such extensive separation were typical, then on typical glaciated bedrock exposures the separation should be recorded by marked abrasion only of the crests of the bedrock highs. This tends indeed to be the case for any bedrock roughness features at wavelengths of a few centimeters, but not for wavelengths of a few meters or many meters. The fact that the ice has the greatest tendency to separate from the bed at wavelengths near λ_α (see section 19) not only reduces the sole roughness at these wavelengths but also reinforces the abrading away of the corresponding bedrock roughness features (section 18), so that the sliding process naturally tends to lead to lower effective roughness near λ_α than at longer wavelengths, and thus to the state of affairs represented by the truncated white roughness spectrum. It is therefore reasonable to find in Table 2 that, for high sliding velocities, the theoretical ζ values for the truncated spectrum are more nearly of the expected size than are those for the white spectrum.

16. SLOPE OF THE BEDROCK SURFACE

The topography described by (3) is superimposed upon a reference plane tilted at the mean slope of the glacier bed; hence, if the roughness is low enough, the bed will slope downstream at all points. The glacier will then be unstable (it could simply slide downhill without any constraint), and the sliding theory developed above would be inapplicable. The low roughness values obtained in Table 2, particularly for the white roughness spectrum, give cause for concern that an unstable state may be implied by the numerical evaluation of the sliding theory.

To investigate this point, we calculate the contribution β of the roughness topography to the over-all slope in the x direction. The local slope contribution is $\beta = \tan^{-1}(\partial z_0/\partial x)$, and for a sine wave $z_0 = a \sin hx$, the maximum slope is

$$\beta_{max} = \tan^{-1} ah \tag{102}$$

If β_{max} exceeds θ, the mean slope of the bed, then upstream-sloping parts of the bedrock surface will be present, and the glacier will be stable. For the general

topography described by (3), it is convenient to calculate the mean square value of tan β

$$\langle \tan^2 \beta \rangle = \frac{A}{4\pi^2} \int_{-\infty}^{+\infty} \iint h^2 a^2(h, k)\, dh\, dk = \frac{4\pi}{3} \int_{-\infty}^{+\infty} \iint \frac{h^2 \zeta^2(h, k)}{l^4}\, dh\, dk \qquad (103)$$

For white roughness, (103) becomes

$$\langle \tan^2 \beta \rangle = \frac{4\pi^2}{3} \zeta^2 \int_{l_1}^{l_2} \frac{dl}{l} = \frac{4\pi^2}{3} \zeta^2 \ln \frac{l_1}{l_2} \qquad (104)$$

In (104) it is necessary to set finite limits on the integration over l, in order to obtain a nondiverging result. Wavelengths over the entire range contribute equally, per logarithmic wavelength interval, to the mean square value of the local slope. Although this might appear to show theoretically that for a white roughness spectrum the glacier can always be stable for any value of ζ, with a suitably wide frequency range l_1 to l_2, in practice the acceptable range of l is limited by the thickness of the meltwater layer between ice and bedrock (a few microns) and by the thickness of the glacier.

Table 3 gives the results of evaluating (102) and (104) on the basis of the roughness results in Table 2. In angle β_m listed in Table 3 is an estimate of the maximum slope angle contributed in the x direction by the bedrock topography (3), and is calculated from

$$\beta_m = \tan^{-1} (2\langle \tan^2 \beta \rangle)^{1/2} = \tan^{-1} [2\pi\zeta(\tfrac{2}{3} \ln \lambda_2/\lambda_1)^{1/2}] \qquad (105)$$

on the assumption that the maximum slope is about $2^{1/2}$ times the rms slope, which is exactly true for the pure sine wave in (102). The wavelength limits $\lambda_1 = 2\pi/l_1$

TABLE 3. Comparison of Mean Bed Slope θ with Estimated Maximum Slope Fluctuations β_m or β_{max}

		White Spectrum			Single Wavelength	
Example	Mean Slope θ, deg	Full β_m, deg	Truncated ($\lambda_L = 3.54$ m) β_m, deg	Long-λ Part β_m', deg	$\lambda = \lambda_\alpha$ β_{max}, deg	$\lambda = 5$ m β_{max}, deg
1	13	18	16	9	18	32
2	13	32	29	17	29	44
3a	28	12	8	6	13	18
3b	28	18	13	9	18	27
4	40	11	11	6	12	23
5	40	36	39	20	32	51
6	3.9	7	6	4	6	10
7	3.9	10	8	5	11	19
8	6.3	29	20	15	32	46
Wavelength limits:						
λ_1, meters		0.002	$5/2^{1/2}$	2	0	0
λ_2, meters		20	$20/2^{1/2}$	20	∞	∞

and $\lambda_2 = 2\pi/l_2$ for the white roughness and truncated white roughness spectra are chosen so as to include a range that is reasonable in relation to typical glaciated bedrock topography. The lower limit λ_1 for the white roughness spectrum is chosen as 2 mm, so as to include only the topography that would be readily visible macroscopically. Because of the similarity of ζ values calculated in Table 2 for the two limiting values of Γ, only the lower value of each pair (for $\Gamma = 77.5$ bar yr m^{-2}) is used in calculating the angles in Table 3. The near equality of β_m and β_{max} values for the white roughness, truncated white roughness, and single-wavelength $\lambda = \lambda_\alpha$ spectra in Table 3 is noteworthy.

The angles β_m and β_{max} calculated from (102) and (105) are compared in Table 3 with θ, the glacier surface slope in each example, which can be assumed a reasonably close estimate of the mean slope of the bed. The examples from valley glaciers (examples 1, 2, 6–8) indicate stability for any of the roughness spectral models evaluated in Table 2. The stability is marginal in example 5, and a definite indication of instability is given for examples 3 and 4; these examples are in icefalls, where the mean slope is high. Because of the peculiar state of affairs at the bed in example 4, as already discussed above, the theoretically derived ζ values are not really appropriate for use in the comparison in Table 3. However, it is little wonder that an indication of instability is obtained; indeed, as an observer of example 4, I found it difficult to conceive that the visible configuration of the sole could actually be stable, although there did exist local upstream-facing slopes on bedrock obstacles that made contact with the sole. The instability shown for example 3 in Table 3 is probably related to the indication, discussed in section 15, that the roughnesses calculated in Table 2 for this example are somewhat too low. The special roughness model discussed in section 15 for this example, consisting of two superposed waves of type (98), each having $a/\lambda = 0.05$ (with wavelengths $\lambda = 10$ cm and $\lambda = 10$ meters), has a maximum slope $\beta_{max} = 35°$, sufficient to give stability.

The angles β_m and β_{max} in Table 3 provide a somewhat independent means of judging whether the bedrock topography defined by the ζ values in Table 2 appears reasonable. On typical glaciated bedrock waveforms several meters in wavelength, the maximum longitudinal slope of the abraded rock surface (disregarding the steep lee sides of roches moutonnées, where the ice separated from the bedrock) is often about 30°, relative to the mean longitudinal slope. With this as a standard of reference, the range of roughnesses indicated for the truncated white roughness spectrum in Table 3 appears reasonable, and that for the single wavelength at $\lambda = 5$ meters either reasonable or somewhat too large. Insofar as we judge the roughness on the basis of what is seen on a scale of several meters, we must correspondingly limit the spectral range over which β_m is calculated from (105) in evaluating the results for the white roughness spectrum; this is done in the column designated β_m' in Table 3, and indicates that the derived roughness is somewhat too low.

17. TRANSITION WAVELENGTH

The contributions of regelation and plastic flow to the sliding process, for a roughness Fourier component of wavelength λ and amplitude a, are given by (37)

and (38), expressed in terms of the amplitudes a_R and a_P by which the sliding ice accommodates the roughness amplitude a through the mechanisms of regelation and plastic flow, respectively. Equations 37 and 38 show that, for short wavelengths ($\lambda < \lambda_0$), the contribution of regelation dominates the sliding process ($a_R > a_P$), and, for long wavelengths ($\lambda > \lambda_0$), plastic flow dominates ($a_P > a_R$). The wavelength λ_0 is at the transition between these wavelength regions of predominating regelation versus plastic flow, and it is therefore called here the 'transition wavelength.'

In the nonlinear sliding theory of sections 10–13, equations 37 and 38 remain applicable, and the contributions of regelation and plastic flow to the sliding process continue to be determined for the individual Fourier roughness components separately. Although the quantity l_0 in (37) and (38) must be replaced by the function $\mathcal{L}(l)$ given by (62), it is possible to recognize a wavelength λ_α that plays essentially the same role as λ_0 in the linear theory. When the definition of λ_α in (69) is appropriate, λ_α is exactly the transition wavelength described above. For other appropriate definitions, as in (80) and (91), l_α is, strictly speaking, the value of $\mathcal{L}(l)$ at that roughness wave number l for which the relative proportion of the regelation and plastic flow contributions has the greatest influence on the sliding process. At this particular l, (37) and (38) are applicable with l_0 replaced by l_α.

To make a detailed evaluation of (37) or (38) for the nonlinear case, it is necessary to introduce the wavelength dependence of $\mathcal{L}(l)$ from (62). For the particular spectrum models discussed in sections 11–13, the needed function $\eta(l^{-1})$ is given by (71), (81), or (95). If, as in section 11, we let $\mu = l/l_\alpha$, with l_α as given by (72), then for the white roughness spectrum we obtain

$$\frac{a_P(\mu)}{a(\mu)} = \frac{X(\mu;\zeta)}{\mu^2 + X(\mu;\zeta)} \tag{106}$$

where X is the quantity that satisfies (74). Similarly for the truncated white spectrum, with $\mu = l/l_L$, we find

$$\frac{a_P(\mu)}{a(\mu)} = \frac{V(\mu;\zeta)}{\mu^2 + V(\mu;\zeta)} \tag{107}$$

where V satisfies (84). For a single-wavelength spectrum, l_α/h is obtainable by solving (96), and a_P/a can then be found from (37), with $l = h$, and with l_0 replaced by l_α.

Figure 6 shows how the ratio a_P/a varies with λ for the white roughness spectrum, according to (106). As ζ becomes large, the wavelength dependence of $\mathcal{L}(l)$ becomes increasingly less pronounced, and in the limit for large ζ the wavelength variation of a_P/a is the same as for the linear theory (constant l_0). The effect on a_P/a of the wavelength dependence of $\mathcal{L}(l)$ is seen to be small, even for the limiting case $\zeta = 0$. The tendency in Figure 6 for the nonlinear plastic flow to make a reduced contribution to the bedrock accommodation, by comparison with that for the linear theory, can be understood in terms of the distribution of viscosity that corresponds to the strain-rate distribution in Figure 2.

In the linear theory it follows from (44) that, for an isotropic roughness spectrum, the contribution to τ from the roughness in any logarithmic wavelength

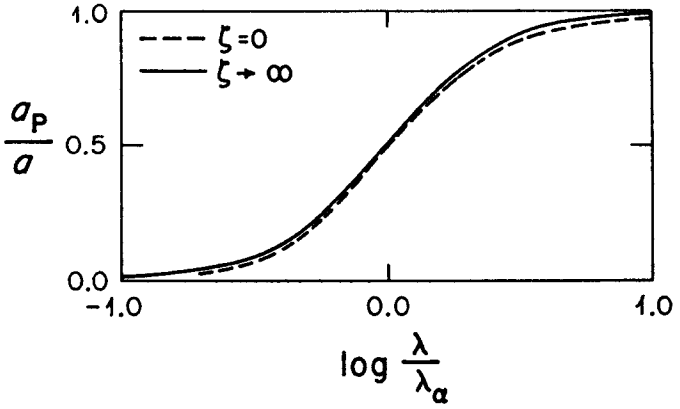

Fig. 6. Ratio of plastic-flow accommodation amplitude a_P to bedrock roughness amplitude a, as a function of roughness wavelength λ relative to the transition wavelength λ_α. The curve for $\zeta \to \infty$ is identical to that for a sliding medium having linear rheology (Newtonian viscosity). The effects of nonlinear rheology are largest for the other limiting case shown ($\zeta \to 0$).

increment $d\lambda/\lambda$ is proportional to $\zeta^2 g(\lambda/\lambda_0)\, d\lambda/\lambda$, where

$$g(\mu) = (\mu + \mu^{-1})^{-1} \tag{108}$$

Since $g(\lambda/\lambda_0)$ rises to a maximum at $\lambda = \lambda_0$, the roughness $\zeta(l)$ at wavelengths nearest to λ_0 can be said to 'control' the sliding motion in the sense that (108) tends to single out the contributions from these wavelengths in determining the resisting stress τ. In the nonlinear theory, from (68), the same conclusion follows, λ_0 being replaced by λ_α as defined in (69).

The quantity λ_α is related to the 'controlling roughness ratio' and 'controlling obstacle size' of *Weertman* [1957, 1964]. From the linear theory in (36)–(38), it is seen that the roughness wavelength, rather than the amplitude (obstacle size) or amplitude/wavelength ratio (roughness ratio), is the fundamentally important parameter of the sliding process. In the nonlinear theory of sections 10–13, λ_α is no longer a material constant, and it shows a dependence on the roughness ζ, but the wavelength remains the basic parameter that determines the resisting stress contribution from (108) or the accommodation contributions from (37) and (38).

For a typical ice viscosity $\eta = 1.3$ bar yr, as measured at the bottom of borehole K in example 1 (Table 1), the transition wavelength λ_0 predicted by equation 42 is 58 cm or 83 cm (for $K_2 = 0.005$ or 0.015 cal sec^{-1} °C^{-1} cm^{-1}, respectively). This prediction agrees with the one existing field observation of features that serve to define λ_0 [*Kamb and LaChapelle*, 1964; example 3 in Table 1]: roughness waveforms at $\lambda \approx 10$ cm were accommodated entirely by regelation, without any detectable plastic flow, whereas wavelengths $\lambda \sim 10$ meters were accommodated by plastic flow with little, if any, regelation.

Transition wavelengths λ_α calculated from the nonlinear theory for the several field examples are given in Table 2. They are obtained from equations (72), (80) + (86), and (96) for the different roughness-spectrum models. In general the calculated wavelengths are distinctly less than what is estimated above from the linear theory, without including the effect of the plastic-flow sliding on η. For field example 3, the λ_α values appear somewhat too small in relation to the observed absence of any significant plastic flow at $\lambda = 10$ cm. This is particularly true for the λ_α values of 17, 22, and 28 cm, which, according to Figure 6, should have allowed a definitely observable amount of plastic deformation at $\lambda = 10$ cm. It was hoped that examples 4 and 5 would provide opportunities for field measurement of λ_α, but the conditions encountered did not make a clear determination possible. In example 4, massive amounts of regelation on a scale of about 35 cm were taking place around a bedrock obstacle making contact with the sole over an area of about the same size, whereas around an obstacle penetrating the ice over an area about 2 meters in diameter, extreme plastic deformation took place on this scale, with local plastic crumpling at wavelengths down to about 25 cm. These observations are consistent with the λ_α values for the truncated spectrum in Table 2, but the λ_α values for the white spectrum and for $\lambda = \lambda_\alpha$ appear somewhat too small. As was explained previously, one cannot place much weight on results derived from the theoretical ζ values (Table 2) for field example 4, because of the peculiar situation at the bed in this locality. In example 5, regelation features were not observable, perhaps because of the high dirt content and the lack of air in the ice; neither could any plastic flow around the obstacles be observed.

For reasons given in section 15, a more detailed discussion of example 3 is justified. If we evaluate λ_α for a single-wavelength roughness at $\lambda = 10$ cm, $\zeta = 0.05$, by solving (96), we find $\lambda_\alpha = 18.3$ or 63.6 cm (for $K_2 = 0.005$ or 0.015 cal sec^{-1} °C^{-1} cm^{-1}, respectively). The marked sensitivity of λ_α to the value of Γ here is noteworthy. A value of 18.3 cm for λ_α is clearly too short; it corresponds to $a_P/a = 0.23$, which would have been readily observed as a warping of the regelation layer. The value $\lambda_\alpha = 18.3$ cm corresponds to a shear-stress contribution $\tau = 1.41$ bar, which is too large. We should use instead a cross-corrugated topography of the type (98), as was done previously, which for the same λ and ζ gives $\tau = 0.50$ bar (for $\Gamma = 155$ (bar yr m^{-2}). In this case, equation 96 must be replaced by

$$\left(\frac{l_\sigma}{h}\right)^{2n/(n-1)} + 2\left(\frac{l_\alpha}{h}\right)^{2/(n-1)} = \left(\frac{\Gamma}{N}\right)^{n/(n-1)} \frac{2\pi}{e}\left(1 + \tfrac{1}{2}\pi^2 e^2 \zeta^2\right)^{1/2} \zeta \frac{v}{h^{(n+1)/(n-1)}} \quad (109)$$

Solution of (109) for the appropriate parameters gives $\lambda_\alpha = 48.2$ or 278 cm (for $K_2 = 0.005$ or 0.0'5 cal sec^{-1} °C^{-1} cm^{-1}, respectively). The quantity a_P/a can be calculated from (38) if we note that for topography of the form (98), $l = 2^{1/2}h$. For $\lambda_\alpha = 48.2$ cm, we find $a_P/a = 0.021$, a plastic-flow contribution that, although definite, is probably small enough to escape detection by observations of the type available in field example 3. It thus appears that the theory is consistent with the observations in example 3, in spite of the indications that λ_α as calculated for the white roughness spectrum, or for a single wavelength at $\lambda = \lambda_\alpha$, is too small.

Direct observations of regelation and plastic flow in the sliding processes, as discussed here and in section 18, provide the most definite quantitative tests presently available for theories of glacier sliding. (The ability of such theories to account for the observed sliding velocities with reasonable roughness values provides a less definite test, first because the high nonlinearity allows great changes in sliding velocity for only modest changes in roughness, and second because the roughness over areas of appropriate size at the bottom of glaciers is presently unknown.) Earlier it was pointed out [*Kamb and LaChapelle*, 1964, p. 170] that the theory of *Weertman* [1957] did not agree quantitatively with observed features of the regelation layer in field example 3. Subsequently, *Weertman* [1964] introduced some modifications into the theory, which affected the numerical results, and he concluded [1964, p. 294] that the theory then gave reasonable agreement with observation. We reconsider this point here. The form of *Weertman*'s [1964] theory is such that the controlling obstacle size, designated Λ, does not depend on the bedrock smoothness ratio s nor on the basal shear stress τ. It is given, from equations (8*b*) and (9) of *Weertman* [1964], by

$$\Lambda = \left(\frac{\beta_\Lambda{}^n}{\gamma^{n-1} bB}\right)^{1/(n+1)} \left(\frac{\alpha C D}{H\rho}\right)^{n/(n+1)} \left(\frac{2}{v}\right)^{(n-1)/(n+1)} \quad (109a)$$

In (109*a*), Weertman's notation is used except for the sliding velocity v. If we follow Weertman in assuming $\beta_\Lambda = 2$, $\gamma = 1$, $n = 3$, $B = 0.017$ bar^{-3} yr^{-1}, $\alpha = 1$, $C = 0.0074$°C bar^{-1}, $D = 0.005$ cal sec^{-1} °C^{-1} cm^{-1}, $H\rho = 73$ cal cm^{-3}, and if we take $v = 5.8$ m yr^{-1} (example 3), we obtain $\Lambda = 2.2$ cm. In the theory, Λ is supposed to be the obstacle size for which regelation and plastic flow make equal contributions to the sliding process; hence, for obstacles of size Λ, the plastic-flow adjustment (corresponding to a_P) should be comparable to the regelation layer thickness (corresponding to a_R). This prediction conflicts with the fact that obstacles of 2-cm size in example 3 showed complete accommodation by regelation, without any observable effect of plastic flow. It thus appears again that Weertman's theory exaggerates the relative contribution of plastic flow to the sliding process for obstacle sizes of a few centimeters. In comparing the predictions of the present theory with Weertman's, the transition wavelength λ_α should be compared with 2Λ, rather than with the 'controlling obstacle spacing' $L' = \Lambda s$ in Weertman's theory, because the distance scale over which plastic flow is assumed to occur in Weertman's theory is Λ, not L'. As was noted earlier, there is a suggestion that λ_α values given by the present theory are somewhat too short, representing some overemphasis on the contribution from plastic flow, but the effect is here less severe than in the predictions of Weertman's theory.

It is not yet possible to make a clear comparison with predictions of Lliboutry's theories. In a recent statement, *Lliboutry* [1969] presents two separate 'controlling sizes' as pertinent to sliding across a pure sinusoidal bedrock profile, but he does not explain the physical significance of these sizes, which would allow a test against observations or a comparison with other theories. The

two sizes stated, 1 meter and 1 cm, lie at the limits of the range of λ_α values found in the present theory.

18. THE REGELATION LAYER

The ice layer involved in the regelation contribution to sliding is a feature that can be observed in the field [*Kamb and LaChapelle*, 1964], and the thickness of the layer can be compared with predictions of the sliding theory. The variable z_R defined by

$$z_R(x, y) = \frac{A}{4\pi^2} \iint_{-\infty}^{+\infty} a_R(h, k) e^{i(hx+ky)}\, dh\, dk \tag{110}$$

represents the local contribution of regelation to the accommodation of the ice to the bedrock topography, and the mean square contribution is

$$\langle z_R^2 \rangle = \frac{A}{4\pi^2} \iint_{-\infty}^{+\infty} a_R^2(h, k)\, dh\, dk \tag{111}$$

If the bedrock topography were a sine wave, the average thickness $\bar{d}_R$ of ice in the regelation layer would be $2^{1/2}$ times $\langle z_R^2 \rangle^{1/2}$ (see Figure 1). We assume that the same factor applies to general roughness spectra. Hence we have from (6), (37), and (111),

$$\bar{d}_R^{\,2} = \frac{8\pi}{3} \iint_{-\infty}^{+\infty} \frac{\zeta^2(h, k)\, dh\, dk}{(l^2 + \mathcal{L}^2(l))^2} \tag{112}$$

In the case of white roughness, and with the simplifying assumption $\mathcal{L}(l) = l_\alpha$ = constant, we find from (112)

$$\bar{d}_R = (\tfrac{2}{3})^{1/2} \zeta \lambda_\alpha \tag{113}$$

For the truncated white roughness spectrum, the corresponding result is

$$\bar{d}_R = (\tfrac{2}{3})^{1/2} \zeta \lambda_\alpha \left(\frac{l_L^2}{l_\alpha^2 + l_L^2} \right)^{1/2} \tag{114}$$

and for a single roughness wavelength λ it is

$$\bar{d}_R = \zeta \lambda h^2 / (h^2 + l_\alpha^2) \tag{115}$$

where ζ in (115) is as defined in (93).

Regelation layer thicknesses, in millimeters, obtained from (113)–(115) with the theoretically derived quantities in Table 2, are given in Table 4. The predicted thicknesses are generally in the range from 1 to 10 mm. The relatively slight decrease in predicted thickness from the white-spectrum model to the truncated white-spectrum model is noteworthy, in view of the fact that the λ_L assumed (3.54 meters) is much longer than the calculated λ_α values.

The regelation layer has actually been observed in field examples 3 and 4, and, possibly, in 2. In example 3 [*Kamb and LaChapelle*, 1964], the maximum thickness was 29 mm. An average thickness was not determined by an averaging

TABLE 4. Calculated Regelation-Layer Thickness for Field Examples

Example	v, m yr^{-1}	$\bar{d}_R$, mm: White Spectrum, Full	White Spectrum, Truncated (λ_L = 3.54 m)	Single Wavelength, $\lambda = \lambda_\alpha$	Single Wavelength, λ = 5 m
1	22.3	2.1	1.2	1.6	0.4
		3.8	2.3	3.0	0.8
2	3.6	8.0	4.8	6.1	1.6
		14.5	9.6	11.0	3.1
3*a*	5.8	4.7	3.2	3.7	1.2
		8.6	6.5	6.8	2.4
3*b*	5.8	5.2	3.4	4.0	1.2
		9.5	6.9	7.4	2.4
4	128.	0.6	0.3	0.4	0.1
		1.0	0.6	0.8	0.2
5	3.6	8.1	4.3	6.1	1.4
		14.6	8.6	11.0	2.9
6	41.	1.8	1.0	1.6	0.4
		3.3	2.1	2.8	0.8
7	41.5	1.0	0.6	0.8	0.2
		1.9	1.2	1.5	0.4
8	3.	7.0	4.9	4.9	1.3
		13.0	9.8	9.0	2.7

The upper and lower values for each entry are for Γ = 155 and 77.5 bar yr m^{-2}, respectively.

of individual measurements, but the average is judged to be about 5 mm. This is in reasonable agreement with the predicted thicknesses in Table 4, except for those from the single-wavelength model for λ = 5 meters. The latter is clearly inappropriate to the observed bedrock topography at the site.

In field example 4, a regelation layer 8 to 14 mm thick was observed at the ice sole, but the source of this layer was inaccessible. The predicted thicknesses (Table 4) are much smaller, but, for reasons noted previously, little weight can be given to the predictions in this case. It appears that the observed regelation layer must have been generated by bedrock obstacles similar in amplitude and wavelength to those observed producing the regelation layer in example 3.

Borehole photography at the bottom of borehole V in example 2 [*Harrison and Kamb*, 1970] reveals a distinct layer about 20 mm thick at the base of the ice, which may be the regelation layer, although positive identification is difficult. The thickness of this layer is somewhat larger than the average thickness predicted in Table 4, but at the point of observation the base of the ice was slightly separated from the bed; hence a maximum thickness, rather than the average thickness, was probably encountered.

The existence of a zone of appreciable thickness over which regelation operates at the base of a glacier must have an important influence on the process of abrasion of the bedrock by rock fragments imbedded in the sole of the moving ice mass. Any rock fragment which, owing to its previous history upstream, extends down into the regelation zone will be forced into severe contact with the crestal part of any bedrock obstacles that project up into this zone. Such obstacles are those for which regelation contributes significantly to the adjustment process in sliding: namely, those having wavelengths of order λ_α and smaller. We can therefore expect that such wavelengths will be removed promptly by abrasion. (This was pointed out previously [*Kamb*, 1964, p. 358].) On glacially abraded bedrock outcrops, this expectation is borne out by the conspicuous scarcity of roughness features at wavelengths less than a few meters. The wavelength λ_α indicated by this evidence is of the order of a meter or somewhat less, consistent with the discussion in section 17.

19. ICE-BEDROCK SEPARATION

The boundary condition used in (21) will be satisfied if at the base of the ice the necessary normal stress distribution $P_0(x, y)$ in (31) is available to keep the ice in contact with the bedrock everywhere. The P_0 in (31) represents a fluctuating contribution that is to be added to the mean pressure σ due to the weight of the overlying ice. If at any point the normal pressure at the base of the ice, equal to $P_0 + \sigma$, were to become negative and hence tensile, the ice would not be able to maintain contact with the bedrock at that point and would separate from it, so that (21) would no longer hold. If a water-carrying passageway in the glacier has access to the bed adjacent to a point where $P_0 + \sigma$ at the ice-bedrock interface becomes less than the ambient water pressure in the passageway, water will intrude along the ice-bedrock contact at this point and ice-bedrock separation will occur. For a large enough water pressure in the passageways, and for large enough fluctuations in $P_0(x, y)$, distributed widely over the bed, it is possible for the areas of ice-bedrock separation to spread out extensively over the bed and to have an influence on the sliding process. This possibility (or something similar) was pointed out and discussed theoretically by *Lliboutry* [1959, 1965, 1968], and has also been considered by *Weertman* [1964]. Since we know, both from observation under glaciers [*Carol*, 1947; *Haefeli*, 1951; *Kamb and LaChapelle*, 1964, 1968; *Harrison and Kamb*, 1970] and from the distribution of abrasion on glaciated outcrops, that the ice does often separate from bedrock, it is important to consider the extent to which this is expected on the basis of the sliding theory.

For a general roughness spectrum, a measure of the fluctuations in $P_0(x, y)$ is, from (49) and (6),

$$\langle P_0^2 \rangle = \frac{16\pi}{3} v^2 \iint \eta^2 \frac{h^2 \mathfrak{L}^4(l)}{l^2(l^2 + \mathfrak{L}^2(l))^2} \zeta^2(h, k)\, dh\, dk \tag{116}$$

If for simplicity we put $\mathfrak{L}(l) = l_\alpha$ in the denominator of (116), then for white roughness (116) gives

$$\langle P_0^2 \rangle^{1/2} = (\tfrac{2}{3})^{1/2} \Gamma \lambda_\alpha v \zeta \tag{117}$$

The normal-stress fluctuations can be compared with the basal shear stress by dividing by (78):

$$\frac{\langle P_0^2 \rangle^{1/2}}{\tau} = \frac{1}{\pi^2(2)} \frac{3^{1/2}}{} \cdot \frac{1}{G(\zeta; n)} \cdot \frac{1}{\zeta} \tag{118}$$

Equation 118 shows that, as the roughness decreases, for fixed basal shear stress, the likelihood of ice separation from the bed increases.

The ice will separate from bedrock wherever $-P_0$ becomes greater than $\sigma - P_W$, where P_W is the ambient pressure of water in passageways having access to the bed. The overburden pressure of ice is given by

$$\sigma = \rho_I g h_I \cos^2 \theta \tag{119}$$

where h_I is the ice thickness measured vertically, and θ is the surface slope. If water in open vertical passageways (such as boreholes) having access to the glacier bed stands at a height h_W above the bed, then the water pressure is

$$P_W = \rho_W g h_W = \kappa \sigma \tag{120}$$

where $\kappa = \rho_W h_W / \rho_I h_I \cos^2\theta$, ρ_W being the density of water. Combining (97), (118), (119), and (120) gives

$$\frac{\langle P_0^2 \rangle^{1/2}}{\sigma - P_W} = \frac{1}{\pi^2(2)} \frac{3^{1/2}}{} \cdot \frac{f \tan \theta}{G(\zeta; n)\zeta} \cdot \frac{1}{1 - \kappa} \tag{121}$$

For the truncated white roughness spectrum, a similar derivation leads to

$$\frac{\langle P_0^2 \rangle^{1/2}}{\sigma - P_W} = \frac{1}{2\pi(2)} \frac{3^{1/2}}{} \cdot \frac{f \tan \theta}{M(\zeta; n)\zeta} \cdot \frac{1}{1 - \kappa} \tag{122}$$

For a single roughness wavelength, the relation between $\langle P_0^2 \rangle$ and τ can be derived immediately from (40) by noting that P_0 and $\partial z_0/\partial x$ are sinusoidal and in phase:

$$\langle P_0^2 \rangle^{1/2} / \tau = 1/\pi 2^{1/2} \zeta \tag{123}$$

Combining (97), (119), (120), and (123) gives, for the single-wavelength case,

$$\frac{\langle P_0^2 \rangle^{1/2}}{\sigma - P_W} = \frac{1}{\pi 2^{1/2}} \cdot \frac{f \tan \theta}{\zeta} \cdot \frac{1}{1 - \kappa} \tag{124}$$

Since we wish to ascertain whether any ice separation from bedrock should take place, we are interested in comparing the maximum value of $|P_0|$ with $\sigma - P_W$. For the single roughness wavelength, the maximum value is $\langle 2P_0^2 \rangle^{1/2}$, and we will assume that the same quantity provides a reasonable estimate of the maximum value of $|P_0|$ for the white roughness and truncated white roughness spectra also. Thus in Table 5 we evaluate the quantity $\langle 2P_0^2 \rangle^{1/2}/(\sigma - P_W)$, from equations (121), (122), and (124), using the data in Tables 1 and 2. The quantity κ is taken to be 0 (no available water pressure) in calculating the numbers in Table 5.

According to Table 5, the sliding theory predicts that ice separation should occur strongly in field examples 3 and 4, to some extent in 5, and not at all in

TABLE 5. Ratio of Maximum Tensile Stress Fluctuation $\langle 2P_0^2\rangle^{1/2}$ to Mean Pressure σ

			$\langle 2P_0^2\rangle^{1/2}/\sigma$			
			White Spectrum		Single Wavelength	
Example	f	tan θ	Full	Truncated (λ_L = 3.54 m)	$\lambda = \lambda_\alpha$	λ = 5 m
1	0.75	0.23	0.95	0.58	1.0	0.56
2	0.75	0.23	0.58	0.39	0.6	0.36
3a	(1.0)	0.53₂	4.0	3.2	4.6	3.3
3b	(1.57)	0.11	4.5	3.35	5.0	3.3
4	0.61	0.84	4.2	2.3	4.8	2.4
5	0.61	0.84	1.5	0.89	1.6	0.84
6	0.5	0.068	0.55	0.34	0.64	0.37
7	0.5	0.068	0.31	0.19	0.35	0.20
8	0.62	0.110	0.21	0.17	0.22	0.13

2 and 6–8, provided that there is no water pressure available at the bed. Example 1 is marginal, in that a little separation may be present if roughness wavelengths near λ_α control the motion, but probably not if the truncated spectrum is applicable.

As a whole, the variations seen in the values in Table 5 are dominated by variations in the surface slope θ from one example to another. As we would expect, the variation is such that glaciers on steep slopes should tend to have extensive separation, whereas those on shallow slopes should not, if water pressure is absent. The ambient water pressure should tend, however, to be greater the gentler the slope, for equal sources of meltwater, and this tends to counteract the decrease in $\langle 2P_0^2\rangle^{1/2}/\sigma$ values for glaciers on gentle slopes.

The predictions of Table 5 correlate with what is known from observation in examples 3 and 4, where there was extensive separation. In example 5, there was only very minor separation (a few cavities about 1 cm high and 4 cm long), which conflicts with the prediction in Table 5, since we know that, for example 5, white roughness is reasonably applicable. This conflict can be explained by the fact that the ice was largely unsupported (owing to separation) over a large area of the bed only about 20 meters from the site of example 5, and hence the normal stress σ at the site was probably higher than is indicated by equation 119. (This explanation would imply some increase also in τ at the site; if this effect were taken into account, the value of ζ calculated from the theory in Table 2 would be increased, and hence the quantity calculated from (121) would be decreased on this account also.)

Borehole photography revealed a separation gap of about 4 cm between the sole and the bed in example 2. This is contrary to the expectations from Table 5, unless one takes into consideration the fact that water in the borehole was standing only 6 to 38 meters below the glacier surface, which corresponds, by (120), to κ = 0.79 to 1.10. Other evidence indicates that the high stand of water in the boreholes was not representative of the ambient water pressure

at the bed, which was probably nearly zero. It therefore appears that the pressurization of a local area of the bed, effected via the boreholes, was responsible for allowing the observed separation gap to form.

An indication that P_w may be significant in examples 6 and 7 comes from the monitoring of water levels in boreholes at this locality [*Raymond*, 1969, p. 88]. The water levels initially stood at the surface, during drilling of the boreholes, but later dropped to depths below about 15 meters. In the best observed instance, the water level in a borehole that reached the bottom dropped and then stabilized at a depth of 40 meters. If the water pressure in a hydraulic system that had access to the glacier bed was sampled, the indicated value of κ in (120) is 0.95. The occurrence of separation is to be judged by comparing $1 - \kappa$ with the quantities in Table 5, and, although a value of κ of 0.95 seems improbably large, on this basis one would conclude that significant ice separation was present in examples 6 and 7.

When the ice had separated partially from bedrock, complications in the heat-flow process at boundaries where the ice has separated will interfere with the exact treatment of regelation sliding in section 5 (particularly equation 9). However, these complications will not be serious for wavelengths at which regelation does not dominate the sliding process. Ice-bedrock separation must cause changes in the form of the roughness spectral function $\zeta(h, k)$, for two reasons: (*a*) separation will tend to occur to the greatest extent at wavelengths near λ_α, because, as can be shown from (116), for isotropic roughness the contribution to the mean-square pressure fluctuation $\langle P_0^2\rangle$ is proportional to ζ^2 (l) g^2 (l/l_α) dl/l (where $g(\mu)$ is given by (108)), and hence for white roughness is a maximum, per logarithmic wavelength increment, at $\lambda = \lambda_\alpha$; (*b*) when the ice separates from bedrock over a distance L, any bedrock roughness features in the interval L are taken out of action, and this tends to reduce the roughness selectively for shorter wavelengths ($\lambda < L$). Both effects *a* and *b* tend to alter the roughness spectrum in the direction toward truncated white roughness. With these limitations, the foregoing theory remains approximately valid for sliding with ice-bedrock separation, provided that the actual bedrock surface is replaced by an imaginary bedrock surface conforming to the ice sole. Thus the inferred ζ values in Table 2 represent effectively the roughness of the glacier sole rather than the actual bedrock. The difference between the two can be significant when there is extensive ice-bedrock separation, as in example 4.

Separation may explain why the ζ values found for examples 6 and 7 (Table 2) appear to be somewhat low. If so, these examples illustrate the occurrence of a significant reduction in effective bed roughness due to ice-bedrock separation made possible by high water pressure. The existence of such extensive separation as would be required to reduce ζ for the sole by, say, a factor of 3 below a bedrock ζ of ~0.05 has not, however, been established by direct observation (except in example 4, where the situation is not at all comparable to 6 and 7). If, in field examples such as 6 and 7, the existence of separation extensive enough to reduce ζ significantly could be established by direct observation, and if the suggested high water pressure at the bed could be confirmed by appropriate measurements over a substantial part of a year, there would then be direct

support for *Lliboutry*'s [1968] emphasis on ice-bedrock separation as an important feature of the sliding process. However, since the present theory is able to account for the high sliding velocity in examples 6 and 7 with bed roughnesses (Table 2) that are not clearly unreasonable, particularly for the single-wavelength spectrum with $\lambda = 5$ meters, the theory does not support *Lliboutry*'s [1965, p. 647] claim that ice-bedrock separation is a necessary condition for the occurrence of high sliding velocities such as the ones in these examples.

When $\langle 2P_0^2\rangle^{1/2}/\sigma$ in Table 5 exceeds $1 - \kappa$, the ice should have separated from bedrock over some portion of the bed area, until the increased mean ice pressure σ' over the part that remains in contact with bedrock is high enough that $\langle 2P_0^2\rangle^{1/2}/(\sigma' - P_W)$ is less than 1. The calculated rms fluctuation of P_0 in this situation is appropriate to the roughness of the sole in the separated condition.

Even when $\langle 2P_0^2\rangle^{1/2}$ is less than $\sigma - P_W$ on the basis of the results in Table 5, one cannot conclude that no ice separation is present at the bed, because the bed may have special roughness features that cause separation but are not reflected in the ζ values inferred in Table 2 on the basis of a white roughness spectrum or the other roughness models. The obvious example is the steep lee side of roches moutonnées, which clearly tends to promote separation, as has been observed under glaciers [*Carol*, 1947] and as is seen from the distribution of glacial abrasion on bedrock outcrops. The ζ values derived in Table 2 represent effectively a roughness spectrum from which the contribution of special roughness features of this type have been eliminated by the separation process itself.

A type of ice-bedrock separation quite different from that discussed above has been proposed by *Weertman* [1962, 1964, 1967, 1969] in a theory of glacier surges. An increase in thickness of the water layer at the ice-bedrock contact is visualized as causing a more or less uniform separation of ice from bedrock over wide areas of the bed. This type of separation is effectively a 'floating' of the whole glacier, which requires a water pressure equal to σ in the basal water layer. If it were to occur, it would, according to Weertman, cause a type of truncation of the bed roughness spectrum, in which obstacles smaller than the thickness of the water layer would be taken out of action in the sliding process. From the viewpoint of the present theory, we would expect that, if the water pressure in the basal layer were caused to approach σ everywhere, there would first occur very extensive local separation in response to the varying local normal stress $\sigma + P_0$ at the bed initially (before separation); only after this extensive local separation had allowed a uniform normal stress σ to develop at the base of the ice could the over-all separation visualized by Weertman begin. For a bed of arbitrary, irregular topography, as visualized in the present theory, existence of a uniform normal stress at the base of the ice would preclude the occurrence of regelation and plastic flow around bedrock irregularities and would require $\tau = 0$; hence it would not be a possible state of affairs in a sliding glacier.

20. CONCLUSIONS

The comparisons in sections 15–19 between features of the basal sliding phenomenon as observed in the field and as predicted theoretically show that the theory in sections 11–13 is able to account reasonably well for the observations.

The roughness values ζ predicted under the assumption of a white roughness spectrum tend to be somewhat lower (by a factor of 2 to 4) than expected from observations of actual bedrock topography, particularly in the field examples of relatively high sliding velocity ($v > 20$ m yr^{-1}). If all the roughness is assumed to be concentrated at the single wavelength λ_α for which the resistance to sliding is the greatest, the ζ values are found to be generally of the expected magnitude ($\zeta \sim 0.05$). However, the resulting model of the glacier bed, a sine wave with wavelength $\lambda \approx 15$ cm, does not closely resemble glaciated bedrock topography as actually observed. Generally reasonable ζ values are obtained alternatively by assuming a truncated white roughness spectrum with lower cutoff wavelength $\lambda_L = 3.54$ meters, corresponding to full roughness ζ developed at wavelengths $\lambda = 5$ meters and longer. Topography with features of the kind represented by this spectrum is typical of glacially abraded bedrock surfaces, and is caused by increased effectiveness of the glacial abrasion process at wavelengths $\lesssim \lambda_\alpha$. For the highest sliding velocities (>40 m yr^{-1}), the cutoff wavelength λ_L for which the predicted ζ values become of the expected size increases to 10 meters or even larger.

From the above relationships it appears reasonable to conclude (1) that the sliding theory in sections 11–13 is quantitatively adequate to account for the observed sliding velocities, and (2) that the typical high sliding velocities (>20 m yr^{-1}) in actual glaciers probably represent sliding over bedrock topography in which roughness at wavelengths up to about 5 meters has been removed by glacial abrasion. The bedrock topography that has been observed under icefalls shows less extensive effects of abrasion and is more appropriately represented by a white roughness spectrum; here the strong tendency for the ice sole to separate locally from the bedrock (section 19) may have an effect on the sliding velocity generally similar to that of truncation of a white roughness spectrum.

For the one field example in which the theoretically predicted transition wavelength λ_α can be compared with direct observation, the λ_α predicted for a white roughness spectrum appears to be somewhat too small, and that for a single roughness wavelength at $\lambda = \lambda_\alpha$ is definitely too small. Although a white roughness spectrum seems appropriate for describing the bed roughness in this field example, it is also possible to describe the bed reasonably in terms of humpy topography of the form (98), with wavelengths $\lambda = 10$ cm and $\lambda = 10$ meters superimposed. This alternative description leads to reasonable agreement with observation; the predicted λ_α values are large enough (48–278 cm) that the expected amount of plastic-flow accommodation at $\lambda = 10$ cm is so small as to be unobservable. Because this alternative description is satisfactory, we cannot conclude definitely that the transition wavelengths λ_α predicted by the theory are somewhat too small, even though the predicted values (λ_α generally in the range from 10 to 40 cm for $v > 20$ m yr^{-1}) are somewhat smaller than the $\lambda_\alpha \sim 1$ meter suggested by the observations in field example 3 and by the typical configuration of glacially abraded bedrock topography (section 18).

Where the regelation layer has been observed in the field, the thickness found has been in the range 0 to 29 mm, averaging perhaps 5 mm. Theoretically

predicted average thicknesses range from about 1 to 10 mm. From (113)–(115), it would be expected that if predicted ζ and λ_α values are somewhat small, the predicted regelation layer thicknesses should be somewhat small also, and there is perhaps a suggestion of this in the comparison between predicted and observed thicknesses. The general agreement, however, is sufficient to establish the conclusion that the effects of regelation extend over a vertical thickness of several millimeters of ice at the base of a sliding glacier.

For low bedrock roughness, the ice will tend to separate from the bedrock in the sliding process; if the roughness is low enough, the ice mass will be unstable. These two effects are related, but they are not mathematically equivalent (sections 16 and 19). Bedrock roughnesses predicted from the theory are mostly large enough to prevent actual instability; the few exceptions are special cases, and allow special explanations. Glaciers sliding on steep slopes tend to have extensive ice-bedrock separation, both as predicted theoretically and as observed in the field. The extent of separation for typical valley glaciers sliding on slopes of less than 15° should be small, according to the theory, provided that water under significant pressure does not have access to the bed. 'Significant' in this connection represents a hydrostatic head amounting to the order of half the thickness of the glacier. Although it is perhaps tempting to explain the somewhat low ζ values as a result of extensive ice-bedrock separation for high sliding velocities, there is no independent observational support for this explanation, and the high velocities (>40 m yr^{-1}) can just as well be explained theoretically by a lack of bedrock roughness at wavelengths $\lesssim\lambda_\alpha$. The extent of separation over special roughness features such as the steep lee sides of roches moutonnées cannot be judged from the theoretically inferred ζ values, because, when there is separation, the ζ values apply to the ice sole rather than to the bedrock itself.

A point of caution in application of the theory must be raised because the predicted maximum strain rates $\dot{\epsilon}_{max}$ implied by the inferred ζ values (Table 6) are considerably larger than the largest $\dot{\epsilon}$ values observed in borehole measurements from which the needed ice-flow law was derived. Little is known about the validity of extrapolating the law flow to such high strain rates. The problem is less severe for the truncated than for the full white roughness spectrum (Table 6).

A field determination of the dependence of sliding velocity v on shear stress τ would be an important test of that feature of the sliding theory that is most important for the over-all flow behavior of glaciers and their response to changing climate. The considerations in sections 10–14 show that the extent of nonlinearity in the response is greatly different for different realistic models of the roughness spectrum, and a field determination would therefore help to discriminate among the alternative models. Not only does the truncated white roughness spectrum give much higher sliding velocities for given roughness ζ, by comparison with a complete white roughness spectrum, but it results also in a more highly nonlinear response, so that the sensitivity of v to changes in τ is greater. From the foregoing results, this greater sensitivity should be expected for valley glaciers with high sliding velocities.

The foregoing conclusions follow from evaluation of the theory with the rather generalized, nonspecific spectrum models represented by white or truncated white roughness, or with the rather over-idealized model of a single roughness wavelength. The theory can, however, be applied to specific examples of bedrock topography, when detailed roughness spectra $\zeta(h, k)$ are measured. To do this, observed roughness coefficients a_{mn}, obtained by Fourier analysis of the topography over a rectangular area of dimensions L_1 by L_2, could be interpolated to give the continuous roughness spectral function $a(h, k)$, and hence $\zeta(h, k)$ from (5), or else the theoretical results in section 10 could be converted to Fourier series form by use of (2) and (2′), and the observed coefficients a_{mn} could then be introduced directly. In either event, it would be necessary to solve (61) with use of the actual roughness spectral function or coefficients, or else to devise a suitable approximation to this solution, along the lines followed in sections 11–13.

Acknowledgments. I wish to thank W. D. Harrison, C. F. Raymond, and J. Weertman

TABLE 6. Maximum Values $\dot{\epsilon}_{max}$ of Strain-Rate Invariant Calculated from Sliding Theory, Compared with Maximum Observed Values

Example	Maximum Observed $\dot{\epsilon}$, yr^{-1}	Calculated $\dot{\epsilon}_{max}$, yr^{-1}: White Spectrum, Full	White Spectrum, Truncated (λ_L = 3.54 m)	Single Wavelength, $\lambda = \lambda_\alpha$	Single Wavelength, λ = 5 m
1	0.60	22.6 15.5	2.6	127.1 84.8	8.3
2	3.1	3.6 2.7	1.0	16.6 11.6	2.7
3a	<0.05	1.1 0.7	0.3	6.7 4.4	0.9
3b	<0.05	2.3 1.6	0.5	13.1 8.8	1.6
4	0.8	169.8 112.6	9.0	>1000.0 684.4	29.5
5	3.5	5.4 4.1	1.8	22.5 16.1	3.9
6	0.045	6.6 4.7	1.6	22.0 15.6	3.5
7	0.054	23.6 15.5	2.1	158.1 102.3	7.1
8	>0.39	2.7 1.9	0.5	22.9 15.4	2.5

Upper values for Γ = 155, lower for Γ = 75.5 bar yr m^{-2}. The observed $\dot{\epsilon}$ values represent shear strain rates at the base of the ice, and one should not expect to equate them with the calculated $\dot{\epsilon}_{max}$ values, which occur at a height $z \sim \lambda_\alpha/2\pi$ or $z \sim \lambda_L/2\pi$ above the bed, and which do not represent primarily a simple shear deformation.

for helpful comments and criticism. Much of the work on which this paper is based was made possible by research support from the U.S. National Science Foundation.

Contribution 1658 from the Division of Geological Sciences, California Institute of Technology.

REFERENCES

Carol, H., The formation of roches moutonnées, *J. Glaciol., 1*, 57, 1947.
Clark, S. P., Handbook of Physical Constants, *Geol. Soc. Amer. Mem. 97*, 1966.
Fletcher, R. C., and B. Kamb, Glacier-flow implications of accurate measurements of borehole length, *Trans. AGU, 49*, 312, 1968.
Haefeli, R., Some observations on glacier flow, *J. Glaciol., 1*, 496, 1951.
Harrison, W. D., and B. Kamb, Direct measurement of sliding velocity at the base of a glacier, *EOS, Trans. AGU, 51*, 431, 1970.
Jaeger, R. M., and D. J. Schuring, Spectrum analysis of terrain of Mare Cognitum, *J. Geophys. Res., 71*, 2023, 1966.
Jahnke, E., and F. Emke, *Tables of Functions*, Dover, New York, 1945.
Kamb, B., The thermodynamic theory of non-hydrostatically stressed solids, *J. Geophys. Res., 66*, 259, 1961.
Kamb, B., An experimental test of theories of non-hydrostatic thermodynamics: AGU, Program 1st West. Nat. Meet., Los Angeles, p. 56, 1963.
Kamb, B., Glacier geophysics, *Science, 146*, 353, 1964.
Kamb, B., and E. R. LaChapelle, Direct observation of the mechanism of glacier sliding over bedrock, *J. Glaciol., 5*, 159, 1964.
Kamb, B., and E. R. LaChapelle, Flow dynamics and structure in a fast-moving icefall, *Trans. AGU, 49*, 312, 1968.
Kamb, B., and R. L. Shreve, Results of a new method for measuring internal deformation in glaciers, *Trans. AGU, 47*, 190, 1966.
Lliboutry, L., Une théorie du frottement du glacier sur son lit, *Ann. Géophys., 15*, 250, 1959.
Lliboutry, L., *Traité de Glaciologie*, vol. 2, p. 640, Masson, Paris, 1965.
Lliboutry, L., General theory of subglacial cavitation and sliding of temperate glaciers, *J. Glaciol., 7*, 21, 1968.
Lliboutry, L., Discussion, *Can. J. Earth Sci., 6*, 940, 1969.
Meier, M. F., and A. Post, What are glacier surges?, *Can. J. Earth Sci., 6*, 807, 1969.
Nye, J. F., On the theory of the advance and retreat of glaciers, *Geophys. J., 7*, 431, 1963.
Nye, J. F., Theory of regelation, *Phil. Mag., 16*, 1249, 1967.
Nye, J. F., A calculation on the sliding of ice over a wavy surface using a Newtonian viscous approximation, *Proc. Roy. Soc., London, A, 311*, 445, 1969.
Nye, J. F., Glacier sliding without cavitation in a linear viscous approximation, *Proc. Roy. Soc. London (A), 315*, 381, 1970.
Raymond, C. F., Flow in a transverse section of Athabasca Glacier, Alberta, Canada, Ph.D. Thesis, Calif. Inst. Technol., 1969.
Savage, J. C., and W. S. B. Paterson, Borehole measurements in the Athabasca Glacier, *J. Geophys. Res., 68*, 4521, 1963.
Sharp, R. P., Glacier flow: A review, *Bull. Geol. Soc. Amer., 65*, 821, 1954.
Weertman, J., On the sliding of glaciers, *J. Glaciol., 3*, 33, 1957.
Weertman, J., Catastrophic glacier advances, *Publ. Assoc. Int. Hydrol. Sci., 58*, 31, 1962.
Weertman, J., The theory of glacier sliding, *J. Glaciol., 5*, 287, 1964.
Weertman, J., An examination of the Lliboutry theory of glacier sliding, *J. Glaciol., 6*, 489, 1967.
Weertman, J., Water lubrication mechanism of glacier surges, *Can. J. Earth Sci., 6*, 929, 1969.

(Received May 20, 1970; revised July 17, 1970.)

REVIEWS OF GEOPHYSICS AND SPACE PHYSICS, VOL. 8, NO. 4, NOVEMBER 1970

Composition and Dynamics of the Solar Wind Plasma

A. J. HUNDHAUSEN

University of California, Los Alamos Scientific Laboratory
Los Alamos, New Mexico 87544

Abstract. Although the coronal origin of the interplanetary plasma implies some general connection between solar and solar wind properties, strong evidence for specific relationships has emerged only recently. Three such relationships will be reviewed here; their observational and theoretical foundations will be discussed, as will their use in determining solar properties from solar wind observations. The first of these involves solar and interplanetary chemical compositions; emphasis will be placed on the implied concentration of helium (and other elements heavier than hydrogen) in the corona. The second relationship to be explored involves the effects of coronal and interplanetary dynamical processes on the properties of the undisturbed solar wind. Arguments for and against the extension of the basic coronal heating process well out into interplanetary space will be developed. The final relationship involves solar activity and properties of the disturbed solar wind. Attention will be focused on interplanetary shock waves produced by solar flares and on implications for the coronal deposition of energy released in flares.

I. INTRODUCTION

The solar wind plays an important role in many phenomena of current interest in space physics. Formed by the continuous expansion of the solar atmosphere into interplanetary space, the solar wind reflects the properties of its source. In particular, solar activity produces characteristic disturbances that are transported by the solar wind throughout the interplanetary region. The solar wind determines the configuration of the interplanetary magnetic field, and thereby controls the propagation of cosmic rays of both solar and galactic origin. The interaction of planetary bodies with the solar wind shapes the magnetic fields and forms the radiation environment surrounding these bodies. The resulting coupling between solar wind properties and many forms of geomagnetic activity provides the final link in the field of solar-terrestrial relationships. The solar wind ultimately interacts with the interstellar medium, maintaining a 'solar cavity' within the galaxy and modifying any interstellar material that attempts to penetrate this cavity.

Wide interest in the solar wind is indicated by the large number of review papers that have discussed basic solar wind properties and phenomena, as well as the interrelationships mentioned above. Recent and comprehensive reviews of solar wind observations and theory have been given by *Dessler* [1967], *Lüst* [1967], *Ness* [1967], *Parker* [1967], *Axford* [1968], *Hundhausen* [1968], *Wilcox* [1968], *Parker* [1969], and *Holzer and Axford* [1970]. The present review will eschew attempted comprehensiveness in favor of a more thorough discussion of